PLACE IN RETURN BOX to remove this checkout from your record.
TO AVOID FINES return on or before date due.
MAY BE RECALLED with earlier due date if requested.

DATE DUE	DATE DUE	DATE DUE

11/00 c:/CIRC/DateDue.p65-p.14

STRUCTURAL ANALYSIS OF A DUCTILE SHEAR ZONE WITHIN THE MARQUETTE IRON RANGE, UPPER PENINSULA, MICHIGAN

By

Cheryl L. Webster

A THESIS

Submitted to
Michigan State University
In partial fulfillment of the requirements
for the degree of

MASTER OF SCIENCE

Department of Geological Sciences

1999

ABSTRACT

STRUCTURAL ANALYSIS OF A DUCTILE SHEAR ZONE WITHIN THE MARQUETTE IRON RANGE, UPPER PENINSULA, MICHIGAN

By

Cheryl L. Webster

The Marquette Synclinorium is interpreted as an asymmetric rift-related basin; truncated stratigraphy on the southern margin and a rollover structure to the north provides evidence for this interpretation. The Palmer Gneiss (PG) marks the southern boundary of the trough. Mining operations have exposed the PG revealing mega-scale shear bands; foliation measurements indicate a reverse sense of shear. The formation of the Palmer Gneiss was previously interpreted as the alteration of the Archean gneiss. Whole rock chemical analysis suggests that the PG rocks are not granitic, but basaltic indicating a Proterozoic age. The folds measured in the adjacent iron formation consistently plunge gently towards the WNW, reflecting that they were formed under the same strain conditions as the shear zone. The NNE-SSW compressive direction is similar to those measured in previous studies of the area. The Penokean Orogeny caused closure of the Marquette trough that reactivated preexisting normal faults and resulted in a reverse dip-slip. Strain was concentrated in a portion of a metadiabase sill that was rotated into the shear zone causing alteration and shearing of the rock to form the PG.

ACKNOWLEDGMENTS

I would first like to thank Cleveland Cliffs Mining Services for supporting me for two summers giving me full access to the mines. Glenn Scott and Helen Lukey's aid was always available and proved very helpful. Thanks also to Paul Nordstrom, Ron Graber, and Tom Waggoner for their support.

Special thanks go to my advisor, Dr. Bill Cambray, for all of his guidance, advice, and most importantly his patience. My committee members, Dr. Tom Vogel and Dr. Kaz Fujita, are also appreciated for their time and their quick review of this thesis. Dr. Lina Patino's help was also gracious and appreciated.

I thank other graduate students for their friendship and insight into life at MSU and beyond. I also thank those students that proved instrumental in finishing this project. In particular, I thank Ed Wilson for being my first field partner, Dave Szymanski for all to the answers to my endless questions, Alexandra de Jong for spending time reviewing several drafts of this thesis, Dave Boutt for the drafting of one of the figures, and also Chris Martinson who was my second field partner.

Finally, I would like to thank my mother and my Aunt Lori for all of their support and giving me a swift kick in the --- when I needed it.

TABLE OF CONTENTS

LIST OF TABLES

LIST OF FIGURES

INTRODUCTION

The Marquette Synclinorium, on the southern margin of the Canadian Shield in the Upper Peninsula of Michigan, is an asymmetric rift-related basin. The trough contains a thick sequence of Early Proterozoic metasedimentary rocks that is situated on Archean basement. The stratigraphy on the southern edge is truncated; a large, low-grade, reverse dip-slip shear zone, mapped as the Palmer Gneiss, marks the boundary between the Archean and Early Proterozoic rocks. The name Palmer Gneiss, representing the Tilden sheared rocks, is misleading because the rock is a phyllite. The shear zone relates to the regional structure; it first acted as a major normal detachment fault during initial extension of the region and was then reactivated as a thrust fault on which the basin inverted.

The Early Proterozoic metasedimentary rocks in the area are known as the Marquette Range Supergroup (MRSG), which lie unconformably on top of Archean gneissic basement. The MRSG is divided into groups separated by unconformities and then subdivided into formal formation units. The oldest part of the sequence is the Chocolay Group, considered to have been deposited in platformal, or possibly basinal, environments associated with the onset of a rifted passive margin (Larue and Sloss, 1980). The Menominee Group unconformably overlies the Chocolay. The deposition of this group occurred along a rifted passive margin in a subsiding basin due to the break up of the continent approximately two billion years ago (Larue, 1981b). The Baraga Group rests unconformably on top of the Menominee Group. Deposition most likely occurred on a deeply submerged and regionally subsiding shelf (Larue, 1981b) or in a foreland basin (Barovich *et al.*, 1989). Associated with the MRSG are numerous metadiabase sills and dikes, which were intruded into the basin during the extension phase.

Approximately 1.9 billion years ago, subsequent to sedimentation of the MRSG, the region experienced a compressional event, the Penokean Orogeny. This event was the result of the Wisconsin magmatic arc colliding with the southern edge of the Superior Craton. The result was closure of the rift-related basin, producing folding and faulting within the MRSG as well as greenschist facies metamorphism. Many workers have investigated the structural history of the area, leading to an understanding of the depositional environments of the MRSG (Larue, 1981a;b), the metamorphism associated with the Penokean Orogeny (James, 1955), as well as strain patterns during deformation (Westjohn, 1990). The purpose of this study is to contribute to the understanding of the regional evolution during the Penokean Orogeny. The major objectives are: (1) to interpret the kinematics of the large, low-grade shear zone, (2) to deduce whether a geometrical relationship between the shear zone and the adjacent folds within the MRSG exists, and (3) to determine the protolith of the sheared rock.

STUDY SITE

Research was concentrated in three areas within the Marquette Synclinorium in the Upper Peninsula of Michigan. Extensive work was completed at the Tilden and Empire mines located in the south-central portion of the trough (N½ Sec. 26, T. 47 N., R. 27 W.; and Sec. 19, T. 47 N., R. 26 W., respectively), and some measurements were taken in the Harvey quarry (NE¼ SW¼ Sec. 1, T. 47 N., R. 25 W.) on the eastern side of the trough (Figure 1).

Both the Tilden and Empire mines are managed and partially owned by Cleveland Cliffs Mining Company. The Tilden has two separate pits, the Hematite and Magnetite pits, but all data were obtained within the Hematite pit (Figure 2). This pit is approximately 1.65 km wide, 1 km long, and 190 m deep. The Empire has five different pits: the Main Pit, CD-I, CD-V, Section 20, and the Southwest Extension; data were collected in the Main pit and the Southwest Extension (Figure 3). The Empire has been operating longer than the Tilden. The Empire, with its five pits, encompass a greater area than the Tilden and the Main pit of the Empire exceeds a depth of 305 meters. The rocks exposed within the mines are Negaunee Iron Formation, metadiabase sills and dikes.

The town of Harvey is located 5 km south of Marquette. Data and samples of a shear zone in the Mesnard Quartzite were collected in a small quarry, just west of US Highway 41.

Figure 1. Location map of study region. Both the Empire and Tilden Mines are located north and west of Palmer, Michigan, respectively.

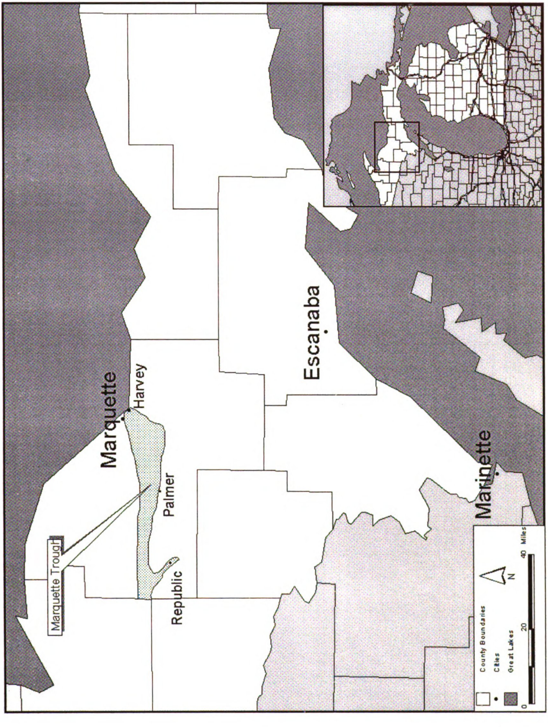
Marquette Trough
Marquette
Harvey
Palmer
Republic
Escanaba
Marinette
County Boundaries
Cities
Great Lakes
N
0
20
40 Miles

Figure 1.

Figure 2. Map of the Tilden Hematite pit. Lines are contours of toes and crests of benches. Benches occur at 45 feet intervals with decreasing elevation towards the center of pit. Arrows represent anticlinal folds indicating the plunge direction and amount of plunge of the fold. Numbers represent the areas studied; area (1) shear zone footwall, (2) hanging wall bench 1440 and 1530, (3) west south wall, bench 1260, and (4) northeast wall benches 1665 and 1710. One inch approximates 550 feet.

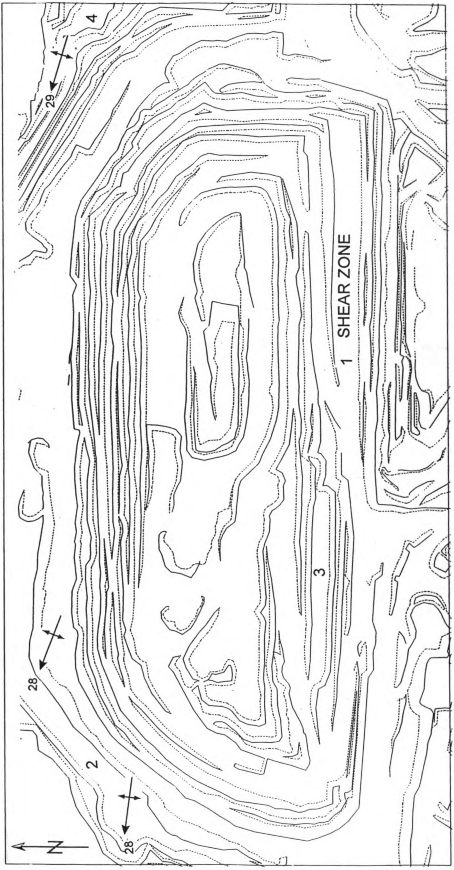

Figure 2.

Figure 3. Map of the Empire Main pit and Southwest Extension pit. Dashed lines are contours of the tops of benches. Benches occur every 45 feet, elevation decreases towards the center of each pit. Arrows represent anticlinal folds indicating the plunge amount and direction of the fold. Numbers represent the areas studied; area (1) northeast corner of SW-Extension pit bench 1215, (2) Main pit Fold One on bench 1080, and (3) Main pit Fold Two, benches 910 and 990. One inch approximates 1100 feet.

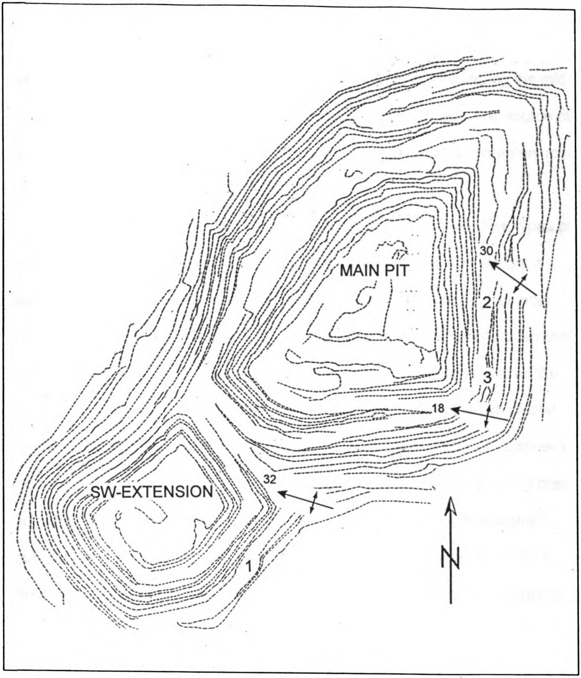

Figure 3.

REGIONAL GEOLOGY

The Lake Superior region, in the southern portion of the Canadian Shield, has undergone billions of years of deposition, erosion, and several episodes of tectonism. Since the discovery of iron ore in the Negaunee area during the mid-nineteenth century, geological interest in the area has continued. The source of the iron ore is banded iron formation (BIF), which is a chemical sedimentary rock that contains more than 15% iron (James, 1954).

The iron formation is underlain by old crystalline basement. Two types of Archean basement rocks compose the craton in the Lake Superior region: a younger (2.7 Ga.) granite-greenstone belt in the north is bounded by an older (3.5 Ga.) gneissic belt to the south (Morey and Sims, 1976). These two terranes were sutured in the Late Archean, and the boundary came to be known as the Great Lakes tectonic zone (GLTZ) of Sims *et al.* (1980). Once the two crustal segments joined, approximately 2.7 Ga, the boundary was a zone of weakness and differential displacement. The two terranes behaved differently during their evolution, the southern gneissic belt did not become tectonically stable until several million years after the granite-greenstone belt was stable (Sims *et al.*, 1980). All of the subsequent Precambrian tectonic activity in the Lake Superior region seems to have been concentrated around the GLTZ, including extension and compression in the more mobile gneissic belt during the Early Proterozoic (Morey, 1993) and during the development of the Midcontinent Rift System.

Tectonic activity in upper Michigan and northern Wisconsin during Early Proterozoic (2.5-1.6 Ga) resulted in the juxtaposition of two terranes, a northern terrane and a southern terrane. The northern terrane contains Archean gneissic basement rocks overlain unconformably by sedimentary rocks of the Marquette Range Supergroup (MRSG). The southern or Wisconsin magmatic terrane is composed mainly of Proterozoic felsic volcanic rocks and calc-alkaline plutons interpreted as an island arc (Sims *et al.*, 1993). The two terranes became sutured together during the Penokean Orogeny, as the island arc collided with the passive margin on the southern edge of the Superior Craton. The Niagara fault is interpreted to be the collisional suture associated with the orogeny (Cambray, 1978; Larue, 1983).

Marquette Range Supergroup

The MRSG is an Early Proterozoic metasedimentary sequence of rock deposited 2.1-1.85 billion years ago (Van Schmus, 1976; Morey, 1983). On the Marquette range, the MRSG consists of three groups; from oldest to youngest these are the Chocolay, Menominee, and the Baraga Group. The Chocolay Group is composed of a basal conglomerate (Enchantment Lake Formation) overlain sequentially by quartzite (Mesnard), dolomite (Kona), and slate (Wewe). Deposition of the group is believed to have occurred in cratonic rift basins (indicated by thick sequences) and on a platforms between the basin areas (thin sequences; Larue, 1981a). Lying unconformably on top of the Chocolay Group is the Menominee Group, which includes the Ajibik Quartzite, the Siamo Slate, and the Negaunee Iron Formation. Deposition is interpreted to have been on a rifted passive margin with the sea located to the south. The Baraga Group, lying unconformably on top of the Menominee Group, consists of the Goodrich Quartzite and an undifferentiated sequence of turbidites, volcanic rocks and iron formations. Deposition most likely occurred on a deeply submerged and regionally subsiding shelf (Larue, 1981b) or in a foreland basin (Barovich *et al.*, 1989). Neodymium isotopes were used by Barovich and others (1989) to determine the source of the sediments within the MRSG. The Lower MRSG has an Archean signature, whereas the Upper MRSG has an Early Proterozoic source, indicating the Baraga Group sediments were shed from the Wisconsin magmatic terrane. Numerous diabase sills and dikes of Early Proterozoic age intruded the MRSG.

Within the study area, the MRSG is mainly constrained by steep-sided, fault-bounded troughs. Many of these troughs are present in the region, including the Republic, Felch, Menominee, and the Marquette trough (MT), which is of particular concern to this study. The basins are all second-order troughs within the larger Animikie Basin (Morey, 1993) and were created by crustal instability within the gneissic basement during a period of extension. The MT, also known as the Marquette Synclinorium, is an east-west trending rift-related basin that extends for 55 km and is approximately 6 km across. The trough is asymmetric with truncated stratigraphy on the southern margin and a more continuous stratigraphic sequence in the north. The thick sequence of sedimentary rock in the trough (approximately 5500 meters) suggests that it was undergoing subsidence during deposition (Larue, 1981a; b). Subsidence was controlled by a normal detachment fault on the south side delineated by the

Palmer Gneiss (Cambray, 1992). As the southern margin of the trough was being uplifted relative to the trough, sediments were shed northward towards the craton. This is evident from the distribution of clastic lenses that increase in thickness and frequency towards the south (Breithart, 1983).

Penokean Orogeny

The Lake Superior region was deformed as a result of the Penokean Orogeny, 1.9 billion years ago (Van Schmus, 1976). The folds developed during this event are characterized by being generally upright to slightly overturned, and doubly plunging. Several reconstructive models of the tectonic episode producing the fold patterns have been proposed. Cannon (1973) argued that the deformation of the Penokean Orogeny was passively induced and resulted from vertical movement of the Archean basement in fault-bounded blocks as the sediments were drape-folded into the troughs. Cannon (1973) also suggested that the second-order basins are best explained by regional gravity sliding of the sedimentary rocks. Morey and Sims (1976) proposed that sedimentation of the MRSG was within an intracratonic basin and that the deposition was followed by intracratonic deformation. Van Schmus (1976) was the first to offer a plate tectonic interpretation, and suggested deposition was on a passive continental margin with the sea extending to the south; deformation subsequently occurred in a back-arc setting with southward dipping subduction. The most accepted model of evolution in the Lake Superior region during the Early Proterozoic is an extension of Van Schmus' idea; Cambray (1978) suggested that sedimentation occurred in rift-related basins along a passive margin that subsequently closed due to a collision of an island arc coming in from the south.

METHODS OF STUDY

Field Methods

Field work was conducted in the summers of 1997 and 1998. The field seasons consisted of measuring bedding and structural features and the collection of rock samples for further petrographic and chemical study.

Accurate measurements of structural features are difficult to obtain in the area because of the magnetic anomalies associated with iron in the rocks. To overcome the limitations of any compass, a new technique was used in the study; an Electronic Total Station (ETS), a survey instrument, was used to avoid the problems of traditional techniques. Other advantages this tool provided are those of accuracy, ease of use, and speed of measurements (Philpotts *et al.*, 1997). For the first time, accurate measurements of deformational features formed in the Early Proterozoic banded iron formation could be measured with this tool.

Measurements in the field were initiated with station point information provided by a mine surveyor. Values obtained from the Global Positioning System (GPS), were given for Easting, Northing, and Elevation based on the mine coordinate system. The mine GPS system is accurate to the sub-centimeter level in all three directions. The Leica (TC 600L) Electronic Total Station (ETS) was set up according to the manufacturer's manual. Once setup, the ETS measures one point at a time; it is not capable of measuring a dip and dip direction of a plane or line. Three points were needed to define a plane and two points to define a line. The reflector was randomly positioned at three places on a particular plane, then measured and recorded. The points for a given plane or line were entered into a program written in Microsoft Excel to convert the Eastings, Northings, and Elevations into a dip and dip direction via solving the "three-point problem." The program was written by W. F. Cambray and modified by Ed Wilson.

Several surveys were conducted at each mine to measure bedding surfaces, axial planes, and hinge lines. The interest of the mining geologists as well as the relative safety of the bench wall controlled the particular areas for field measurement. At the Tilden, four areas were surveyed: (1) Shear zone footwall on the east south wall of the Hematite pit, benches 1305 and 1440, (2) North hanging wall on benches 1440 and 1530, (3) West south wall on bench 1260, and (4) North east wall on benches 1665 and 1710 (Figure 2). At the Empire mine, surveys were conducted in the Southwest Extension pit on bench 1215, and also on the north and east side of the Main pit on benches 910, 990, and 1080 (Figure 3). Approximately 1000 planes and lines were measured throughout both summers and mines.

Samples of rock in the area were collected for petrographic and chemical analysis. At the Tilden mine, four oriented samples (#1-4) were collected outside the Hematite pit on its eastern side. These rocks are sheared, however, appear to have experienced less strain than the rocks in the main part of shear zone. Three oriented samples (#5-7) of the Palmer Gneiss were collected outside of Empire mine property (Sec. 23, T47N, R27W). Examples of the metadiabase sill (#8-10) within the Tilden were taken. Number 8 was the freshest sample (furthest from the shear zone), and samples 9 and 10 were progressively more altered and closer to the shear zone. Oriented samples (#11-12) were collected from the Harvey quarry. Samples #13-22 (#13-15 oriented) were collected on the Tilden shear zone wall. During a field trip to the Tilden Mine in May 1999, more samples of the shear zone were collected along with samples of metadiabase, and Southern Complex Gneiss.

Lab Methods

Chemical analyses of the rocks from the high and low strained parts of the shear zone, the diabase sills, the Palmer gneiss, and Southern Complex gneiss were performed with an automated X-Ray Fluorescence Spectrometer (XRF). Whole rock major elements, as weight percent oxides, and trace elements were determined from homogenous glass wafers. Wafers were made by combining 3 g of finely ground rock powder, 9 g of lithium tetraborate (flux), and 0.5 g ammonium nitrate (oxidant) and heated in a platinum crucible at approximately 1100 °C for 20 minutes. After that time, the homogenous mixture was poured into a platinum mold and quenched.

Petrographic analyses were conducted of the Tilden sheared rocks, the metadiabase from the Tilden, and also one from the Mesnard Quartzite in the Harvey quarry. Oriented thin sections, cut perpendicular to foliation and parallel to lineation, were made on samples 1, 2, 3, 4, 5, 12, 14, and 15. Randomly oriented thin sections were cut from samples 8, 9, and 10. Microkinematic analysis of the sheared rocks was used to support observations made in the large shear zone. Following Simpson and Schmid (1983), three prospective types of kinematic indicators were investigated for, (1) rotated porphyroclast tails and asymmetric pressure shadows, (2) fractured and displaced grains, and (3) asymmetry of quartz crystallographic fabrics.

SHEAR ZONES

Shear zones form through crustal deformation and can occur under brittle, ductile, or any intermediate conditions. Shear zones developed under brittle conditions will form close to Earth's surface and show fractured features (Twiss and Moores, 1992). Ductile shear zones form at a depth of approximately 10-15 km, where the strain is accommodated by strain softening and crystal-plastic deformation (White *et al.*, 1980). Intermediate conditions result in features having both characteristics of ductile and brittle deformation (Twiss and Moores, 1992). The shear zones in the Tilden Mine and the Harvey quarry were deformed through ductile deformation, in that the differential displacement in the shear zone was controlled by ductile flow, thus layers may have changed shape but did not break apart (Ramsay, 1980).

An ideal shear zone has parallel sides and contains identical displacement throughout the zone. The displacement field within the shear zone is simple shear and/or volume change (Ramsay, 1980). Simple shear is a rotational strain compared to pure shear that is a nonrotational, homogeneous strain. During pure shear, the Z-axis or the maximum shortening direction is oriented perpendicular to the shear zone, and the X-axis or the maximum elongation direction, is aligned parallel to the shear zone (Figure 4a). The orientation of the strain axes is the same for an instantaneous amount of strain as well as for finite strain, thus deformation is coaxial. An instantaneous strain ellipsoid of simple shear (Figure 4b) shows that the maximum elongation direction (X-axis) is oriented 45° to the shear plane.

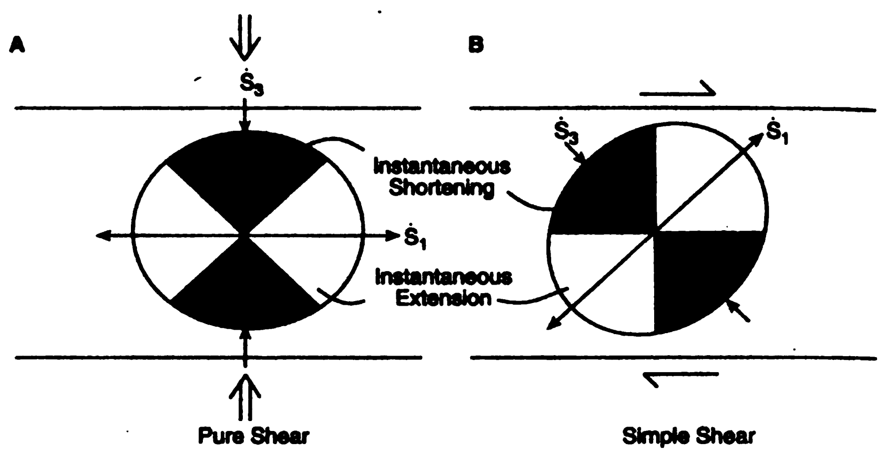

Figure 4. Instantaneous strain ellipsoids of pure (A) and simple shear (B).

However, as shear increases, the X-axis rotates towards parallelism with the shear zone, as the Z-axis rotates normal to the shear plane. The finite strain ellipsoid is different than the infinitesimal strain ellipsoid, hence, simple shear deformation is noncoaxial.

Because simple shear is a basic component of many shear zones (Ramsay, 1980), one side of the shear zone is displaced relative to the other. Shear sense indicators or kinematic indicators are often preserved in the shear zone to determine this relative displacement. Useful types of indicators include grain tails, mica fish, S-C fabrics, and shear bands. The latter two indicators are of particular interest because they are both observed in the shear zones studied.

S-C fabrics and shear bands are types of foliation patterns. An isotropic and homogeneous material undergoing simple shear stress will result in the formation of the S-foliation. This foliation is a preferred orientation of the grains that is parallel to the XY plane of the finite strain ellipsoid, see Figure 5 (Ramsay and Graham, 1970). As shear increases in the zone, the S-foliation continually rotates towards parallelism with the shear wall, and may become indistinguishable from the C-foliation, which parallels the shear zone boundary. The geometry of S-C fabrics in a dextral shear zone is illustrated in Figure 6a; the acute angle of the S-foliations point in the direction of shear, and the C-foliations are evenly spaced breaks that help accommodate the strain (Platt, 1984). It remains uncertain as to whether S- and C-foliations form simultaneously (Lister and Snoke, 1984), however, Platt (1984) refers to these foliations as a primary fabric, ductile shear bands form as a secondary fabric. Shear bands (denoted as

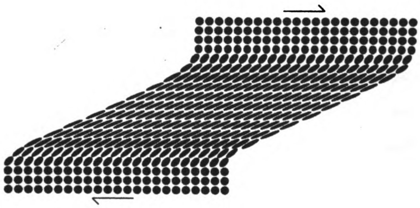

Figure 5. Diagram of heterogeneous strain in a dextral shear zone. The initial circles become elongate and align themselves in the X-Y plane of finite strain ellipsoid.

a.

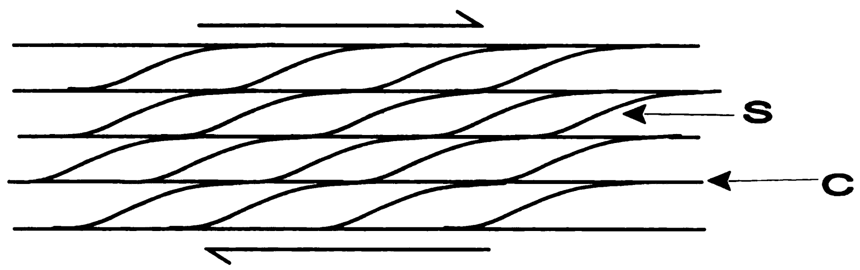

b.

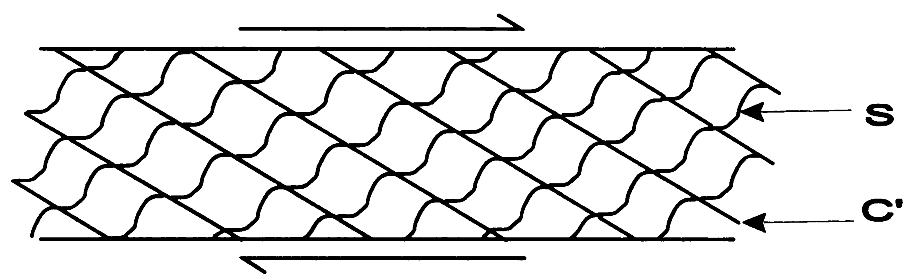

Figure 6. S-C structures (a) and shear bands (b) in a dextral shear zone. Note the C-foliations are parallel to the shear zone and the shear bands are at an angle to the zone boundary.

C') are also known as extensional crenulation cleavages. The geometry of shear bands in a dextral shear zone is shown in Figure 6b, which shows that the S-foliation is broken up by the C'-foliation. Shear bands occur at an angle to the shear wall. The effect of shear bands is to extend the foliation by ductile normal faults, in effect, they are small shear zones within a shear zone (Platt and Vissers, 1980).

Tilden Shear Zone

The stratigraphy on the southern margin of the Marquette Synclinorium is truncated; the Palmer Gneiss (PG) demarcates the boundary between the Archean (Southern Complex) gneiss and the Early Proterozoic metasedimentary rocks of the MRSG. Van Hise and Bayley (1895) first interpreted the PG as a pulverized, sericitized, and partly silicified phase of the Lower Precambrian gneiss. Through extensive mapping, Gair and Simmons (1968) concurred with the previous interpretation and concluded the PG to be an altered rock, an example of retrograde metamorphism. Since 1968, open pit mining operations at the Tilden Mine have exposed the rocks that mark the trough boundary, and have revealed large shear bands that indicate the importance of ductile deformation during its alteration. For the first time, the exposure also allows a chance to study the shear zone and obtain reliable data to characterize the orientation of the last movement along this fault.

Geometry of the Shear Zone

In the shear zone, two distinct foliations are recognizable, the S and the C′-foliation. All foliation surfaces were measured along two different benches on the south wall of the Tilden Hematite pit. The S-foliations are larger, more pronounced, more abundant, and easier to measure than the shear bands, which were both less abundant and less accessible than the S-foliations; therefore fewer measurements were taken. A list of all measurements can be found in the Appendix A, Table 1. The steep S-foliation gently curves into the C′-foliation with spacing between the two approximating 2.5 meters (Figure 7). The geometry of the shear bands (Figure 8) indicates a reverse sense of motion. To determine the precise orientation of the reverse motion, the orientation of the S-surface, the shear bands, their intersections and the top of the shear zone boundary are compiled on a stereonet (Figure 9). The S-foliation steeply dips to the NNE, and the C′-foliation shallowly dips to the NNE. A plane perpendicular to the intersection of the S and C′ represents the plane of motion of the shear zone. To obtain the actual slip direction, the shear zone boundary is necessary. Since the boundary between the shear zone and the MRSG has been removed by mining, the top boundary was reconstructed from maps and models generated by the mining company. The actual slip line is determined by the intersection of the shear zone boundary and the plane normal to the S-C' intersection, and was calculated to be 046/58. The principal shortening direction is NNE-SSW.

East of the Hematite pit, a small outcrop is exposed showing a cross section through part of the PG. The outcrop contains mesoscale S-C structures

Figure 7. Photograph of the Tilden shear zone. The steep foliation is the S-foliation, notice it curves into the shear band, shallower dip. The spacing between the shear bands approximates 2.5 meters.

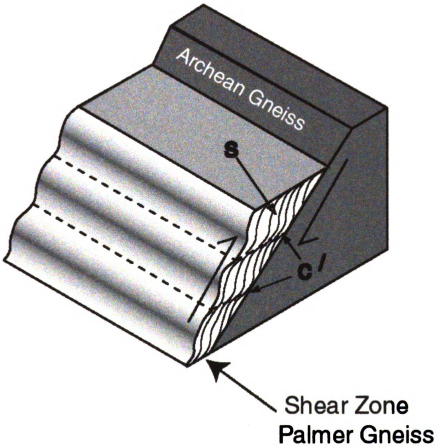

Figure 8. Diagrammatic sketch of the Tilden Footwall, note the steep S-foliation curving into the shear band indicating a reverse sense of motion.

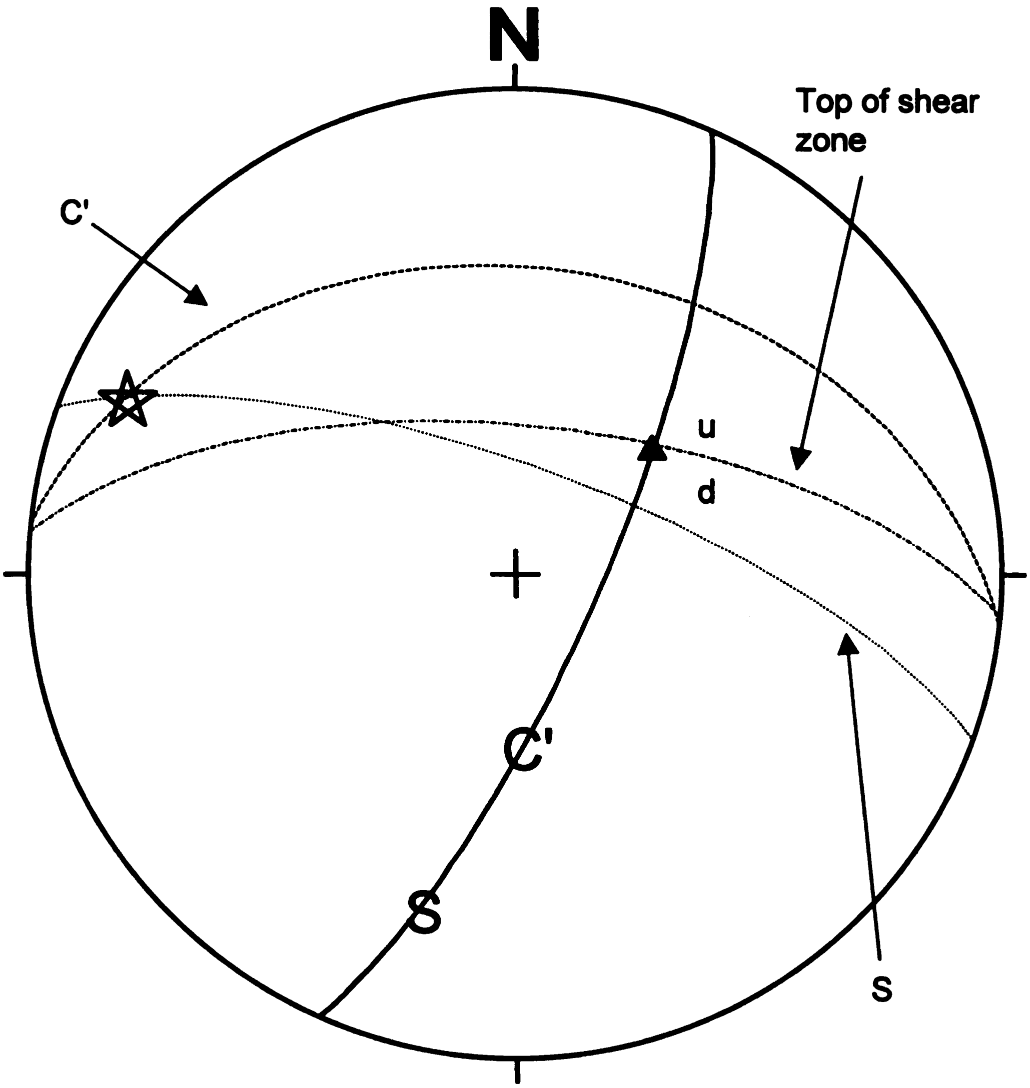

Figure 9. Stereonet plot of the Tilden shear zone. The C' is the mean pole to the shear bands, the mean C' plane is the dashed line. The S is the mean pole to the S-foliation with the dotted line as the mean S plane. The star indicates the mean intersection of the C' and the S plane; solid line is the plane perpendicular to this S-C' intersection. The long and short dashed line is the top of the shear zone; triangle represents the plunge of the line of movement of 046/58. As it is a reverse shear zone, the movement was up towards the SSW, u is the upthrown, d is the downthrown side.

that indicate a reverse sense of motion. The S-foliations are steeply dipping towards the NNE, and the C-foliations dip to the NNE with a shallower dip (Figure 10). The plane perpendicular to the S-C intersection along the C plane indicates the movement direction, 048/49. The S-C structures support the large shear bands located in the Hematite pit, and suggest a NNE-SSW compressive direction during reverse dip-slip.

Petrography and Kinematic Analysis

Petrography was conducted to observe the mineralogy, texture, and fabric of the sheared rock as well as the protolith. Thin sections were prepared on two oriented samples from the Tilden shear zone and on three, non-oriented samples of metadiabase. The samples of metadiabase were collected progressively farther away from the shear zone, the furthest representing the 'freshest' sample.

The Tilden sheared rocks have a very well developed foliation. The mineral assemblage is mainly chlorite with some opaques (hematite, magnetite), quartz, and a few grains of tourmaline. The opaques are subhedral, fine to medium-grained and concentrated along planes of foliation. The quartz is generally fine grained and displays undulatory extinction. Figure 11 shows the well-foliated texture of the sheared rocks. No microscale kinematic indicators were found. Strain was concentrated in the development of the large shear bands.

The petrography of the metadiabase is quite similar to the Republic dikes described by Weaver (1994). The 'freshest' sample is medium to coarse-grained

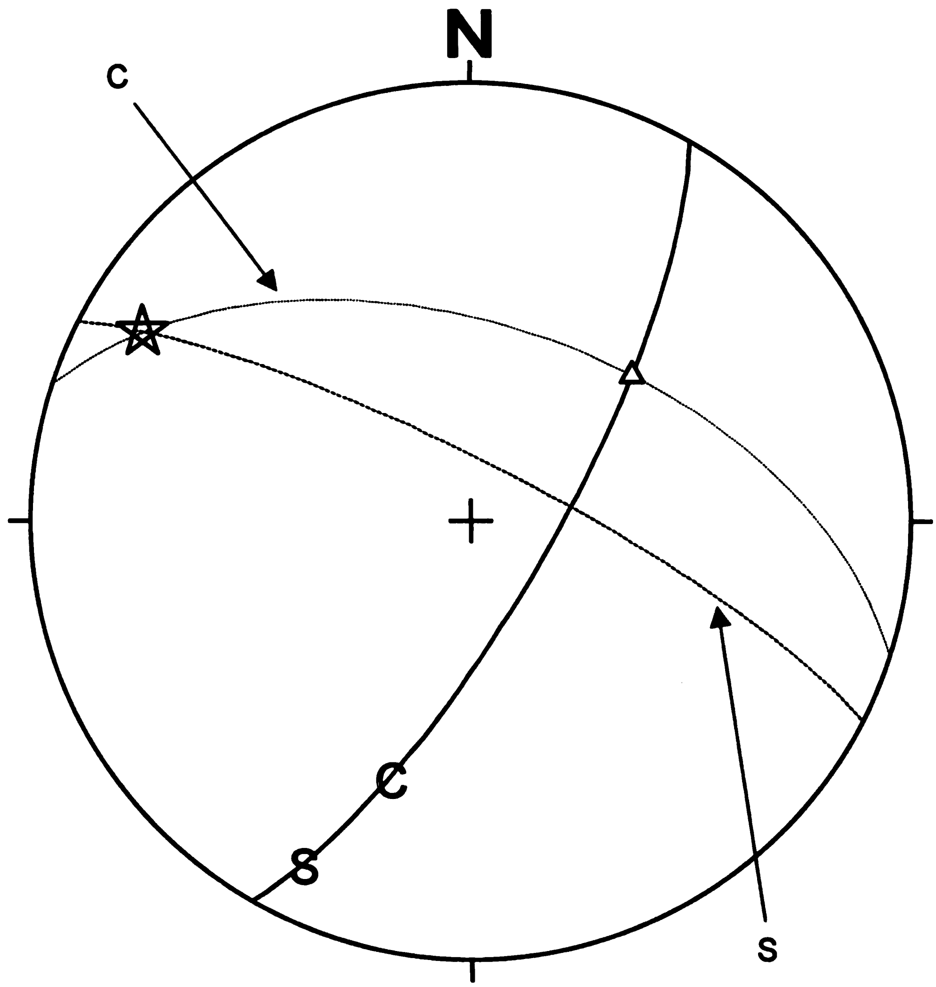

Figure 10. Stereonet plot of S-C structures outside of the Tilden Hematite pit. C represents mean pole to the C-foliation, short dash line is the mean C-foliation. The long dash line equals the S-foliation, and the S is the pole to that plane. Star indicates the mean S-C intersection and the solid line is the plane normal to the intersection. Triangle is the plunge of the line of movement.

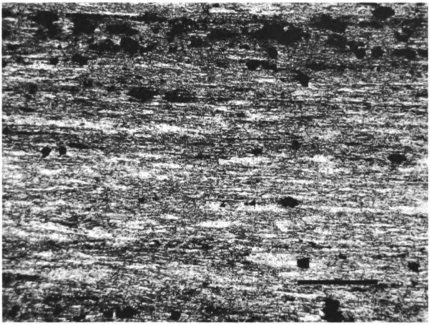

Figure 11. Photomicrograph of the Tilden sheared rock (PG). Notice the well developed foliation. Scale bar equals 0.5 mm.

and contains mainly plagioclase, amphibole, biotite, with minor amounts of chlorite, epidote/clinozoisite, and magnetite-ilmentite. The plagioclase is twinned, altering to sericite, and is subhedral. The amphiboles are the alteration product of the original pyroxene, they show yellow to blue-green pleochroism, and are also subhedral. The opaques are mostly euhedral, however, they are partially exsolved away. The metadiabase samples become progressively finer grained as the samples get closer to the shear zone; the mineralogy of the samples becomes unidentifable.

Harvey Shear Zone

The Marquette trough is a large, east-west trending synclinorium that extends eastward to Lake Superior. The stratigraphy on the eastern margin, above the Archean pillow basalt, consists of the Enchantment Lake Formation, the Mesnard Quartzite, and the Kona Dolomite. The outcrop in the Harvey quarry reveals the north dipping southern limb of a syncline; approximately 100 meters outside the quarry the northern limb dips to the south (Figure 12). A ductile shear zone is observable in the quarry and is contained within the Mesnard Quartzite at the contact with the Archean basement. The shear zone contains clearly recognizable, mesoscale, shear bands (Figure 13).

Geometry of the Shear Zone

The ductile shear zone, bounded by less strained quartzite, is nearly 1 meter in width and contains the distinguishable foliations, S and C′. Similar to

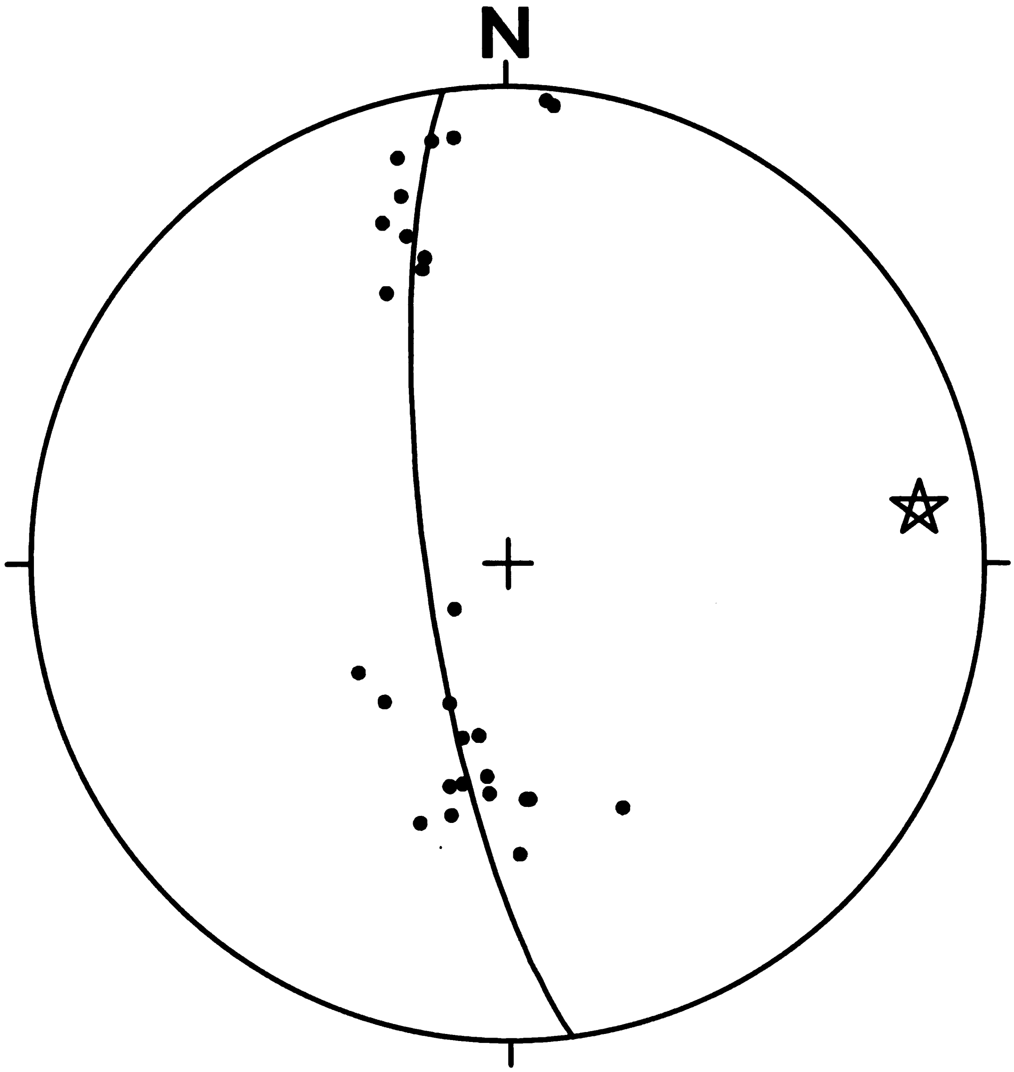

Figure 12. Stereonet plot of a syncline in the Kona Dolomite and the Mesnard Quartzite exposed in the Harvey Quarry. Circles are the poles to bedding surfaces with a best fit great circle; the star represents the fold axis gently plunging to the ENE.

Figure 13. Photograph of the shear zone in the Harvey quarry. The line labeled C′ illustrates the orientation of the shear band, the line marked S parallels the S-foliation.

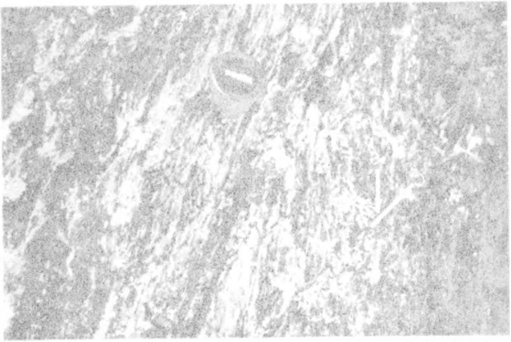

the Tilden shear zone, the S-foliations curve into the shear bands, and they steeply dip to the NNW while the C′-foliations shallowly dip to the NNE (Figure 14), see Appendix A, Table 2 for measured data. The spacing between the two foliations is approximately 10 cm. The geometry of the shear bands indicates a reverse sense of motion. The intersection of the shear zone boundary with the plane perpendicular to the S-C′ intersection results in a slip direction of 316/48. This area of high strain formed under a NNW-SSE compressive direction, different than the Tilden shear zone, it is an angle normal to the boundary of the trough reflecting local variation in the stress field.

Petrography and Kinematic Analysis

One thin section was prepared from the shear zone in the Mesnard Quartzite to analyze for kinematic indicators. The mineralogy is comprised of fine-grained white mica (sericite), quartz, and opaques (hematite). Similar to the Tilden sheared rocks, the sheared rocks in the Harvey quarry are also well foliated, separated into zones of quartz and zones of fine-grained quartz plus sericite. The opaque porphyroclasts acted as rigid objects during deformation producing an inhomogeneous strain pattern around the crystal resulting in pressure fringes (Spry, 1969). These pressure fringes can be used as kinematic indicators, however, they are complex and did not form part of this study. Mesoscale shear bands are also observed in the rock and are distinguished by the fine mica cutting across the preferred quartz direction representing the S-

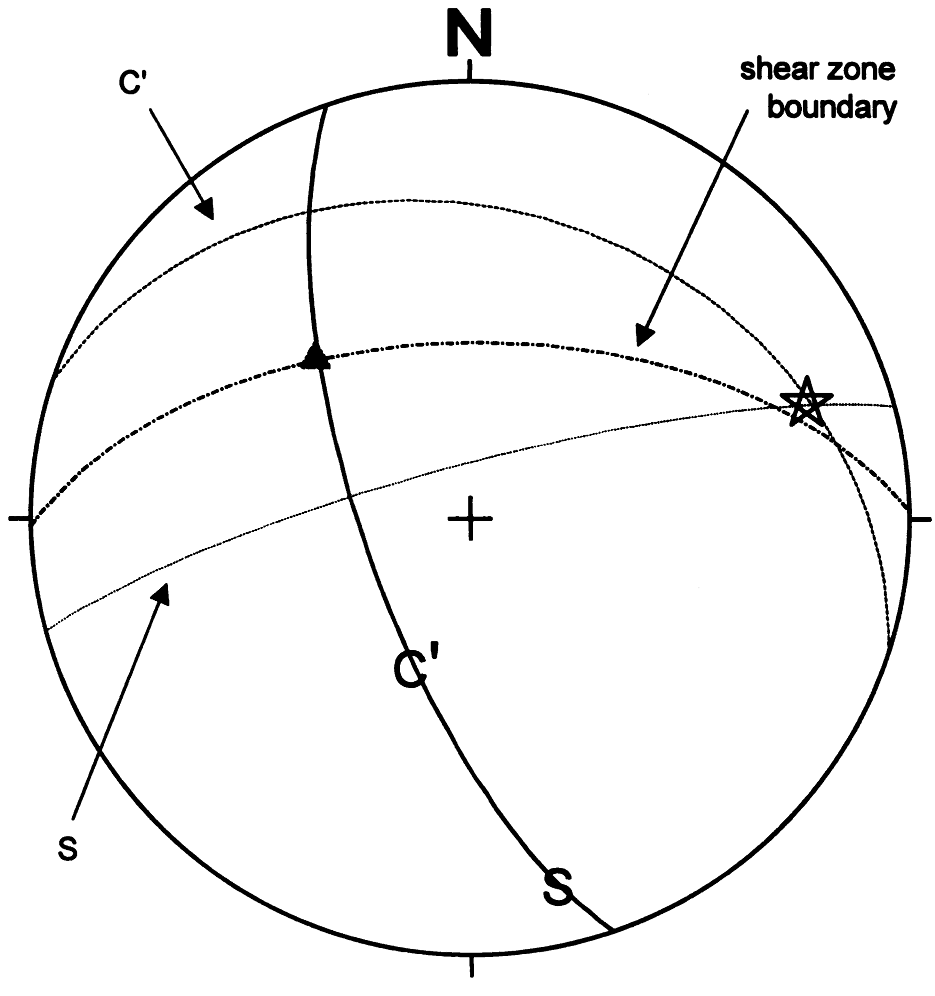

Figure 14. Stereonet plot of the Harvey shear zone within the Mesnard Quartzite. The C' is the pole to the mean shear band with the dashed line as the mean C' plane. The S is the pole to the mean S-foliation with the dotted line as the mean S plane. The star represents the intersection of the S-C' planes and the solid line is the plane normal to that intersection. The long and short dashed line is the shear zone boundary; triangle represents the movement direction of 316/48.

foliation. These indicators also suggest a reverse motion supporting the mesoscale shear bands.

FOLD GEOMETRY IN NEGAUNEE IRON FORMATION

The Negaunee BIF lies adjacent to the Tilden shear zone and is an extensive unit within the Marquette Synclinorium. The iron formation has been deformed into many folds observable at the Tilden and Empire Mines. The exposure of the open pit mines allows for great accessibility to the folds. Measurements along several walls were used to define some of these folds to determine if a geometrical relationship exists between the folds and the shear zone in order to deduce whether the deformation of the two occurred under the same stress conditions. Data was collected mainly on bedding, but hinge lines and axial surfaces of drag folds were also measured. Fold axes are determined from stereonet plots; the pole of the best-fit plane through the poles to bedding was used to define the fold axis. All of the following data is plotted on an equal area stereonet using StereoNet version 3.0 for Windows (Steinsund, 1995).

Tilden Mine

North Hanging Wall

In the Hematite pit, measurements were obtained on the north side of the pit and on the northeast side of the hanging wall; a haul road that connects to the Magnetite pit separates these two areas (see Figure 2). On the north side, data was restricted to two benches, 1440 and 1530. The upper bench was directly above the other, but less data was obtainable due to poorer, and smaller exposure and the presence of intrusives. Measurements included 138 bedding planes, 22 axial planes, and 17 hinge lines for the lower bench and 17 bedding planes, four hinge lines and axial surfaces for the upper bench (see Appendix A, Table 3).

A stereonet plot of the measurements is shown in Figures 15 and 16, and represents the benches 1440 and 1530, respectively. The axial surface plane represents a mean value of those planes measured. The small drag folds, which represent the larger fold, were used to measure hinge lines directly or by projecting the line out of the wall face. Axial surfaces were determined by aligning a clipboard adjacent to the axial surface and measuring the board. This method resulted in some error, which explains why many of the hinge lines do not fall directly on the axial surface. The geometry of the fold is consistent on both benches; the poles to bedding conform to a great circle with a fold axis gently plunging around 28° towards the WNW, subparallel to the trend of the trough. The axial surface dips to the NNE, indicating the folds are overturned to the SSW; the hinge line plunges 30° towards the WNW. The orientation suggests that this fold, illustrated on two benches, formed under a NNE-SSW compressive direction.

Northeast Hanging Wall

A metadiabase sill is the prominent rock type in the upper northeast side of the hanging wall. Joint orientations were the key measurements made in this area, except data were obtained for a mine geologist and are not a concern to this study. However, bedding, hinge lines, and axial surface information in the iron formation was available and attained. Measurements on bench 1710

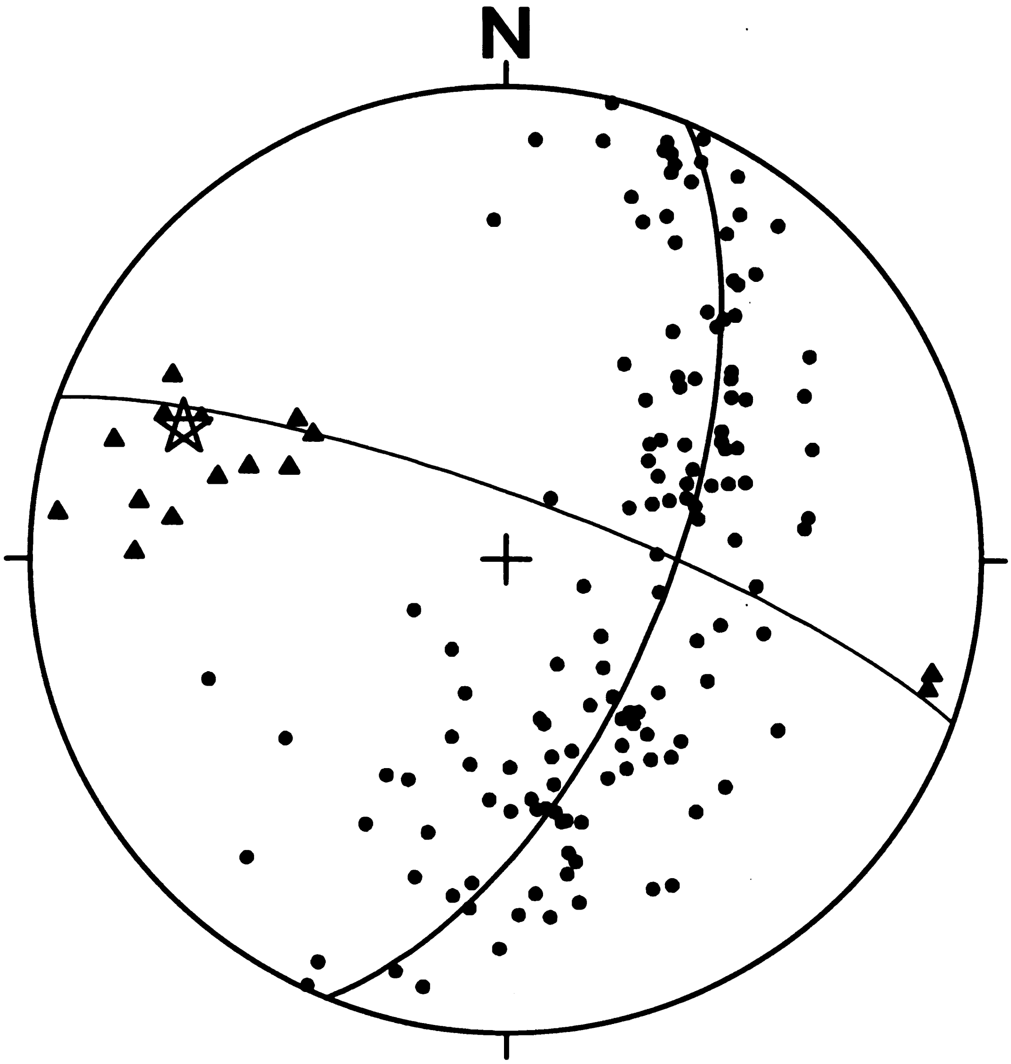

Figure 15. Stereonet plot of the fold on the Tilden Hanging Wall bench 1440. The circles are poles to bedding with a thick line representing the best fit great circle. Fold axis (star) is plunging to the WNW, triangles are the measured hinge lines and the thin line shows the mean axial surface dipping to the NNE.

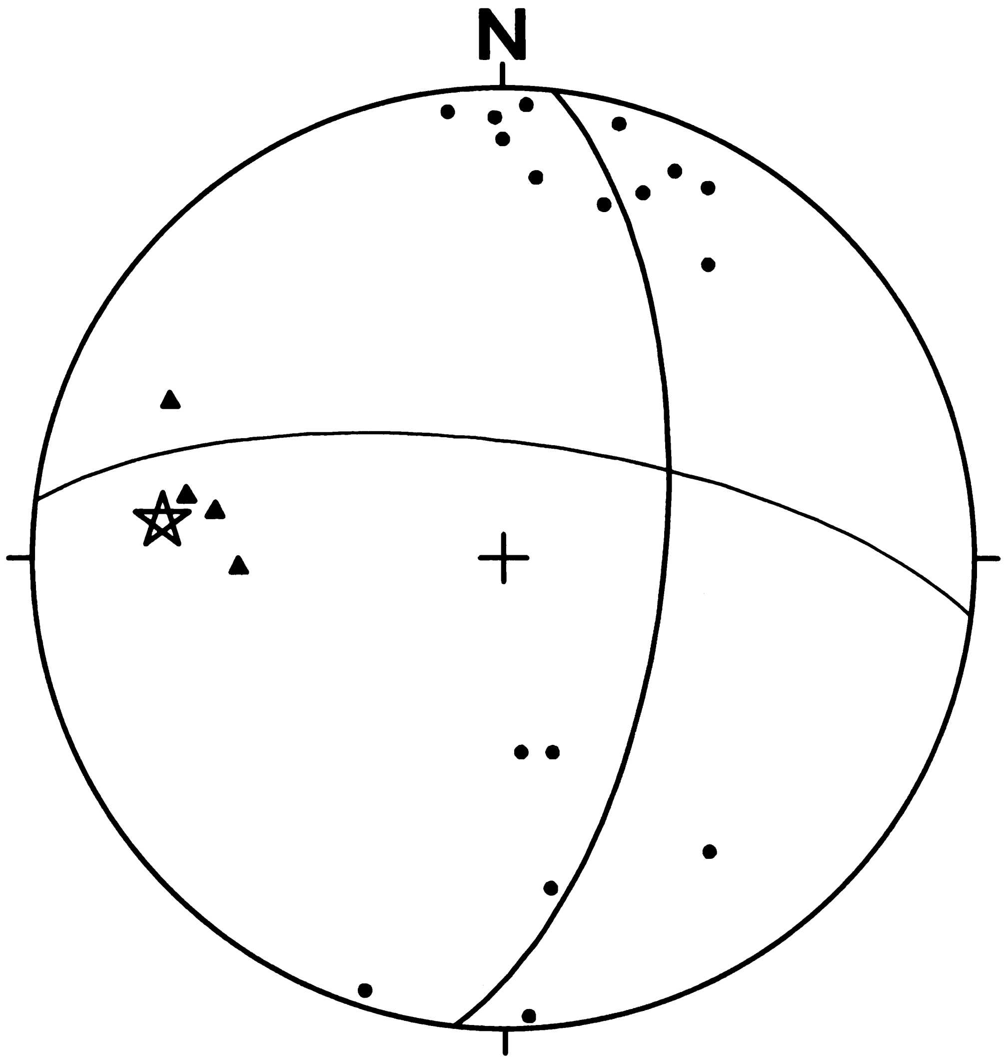

Figure 16. Stereonet plot of the Tilden hanging wall bench 1530. Poles to the bedding are the circles, thick line is the best fit great circle about the bedding poles. The star is the fold axis plunging to the WNW. The thin line indicates the mean axial surface, and the hinge lines are represented by the triangles.

included 35 planes of bedding, 6 hinge lines and 3 axial surfaces (Appendix A, Table 4).

A summation of the geometry is shown on a stereonet plot, Figure 17. The poles to the bedding congregate about a great circle with a fold axis plunging towards the WNW. The hinge lines are also plunging in the same direction and with the same approximate dip as the axis. The mean axial surface is steeply dipping to the NNE. Geometry suggests a NNE-SSW principal shortening direction.

Empire Mine

Southwest Extension

An anticline is exposed on the northeast side of the Southwest Extension pit. The rocks within this part of the pit are the Negaunee BIF and the Siamo Slate. The BIF contains many small drag folds whereas the slate is more massively bedded and contains no minor folds. Measurements were taken in both formations and started with the 1215 bench and moved up ramp on a main haul road.

Figure 18 is a stereonet plot of measured data of the anticline. Data included 152 bedding measurements, 5 hinge lines and 5 axial surfaces (Appendix A, Table 5). The poles to the bedding are distributed in a great circle with the fold axis gently plunging at 32° to the WNW. The axial surface dips steeply to the NNE and the hinge line plunges shallowly to the WNW. A principal shortening direction of NNE-SSW produced this fold.

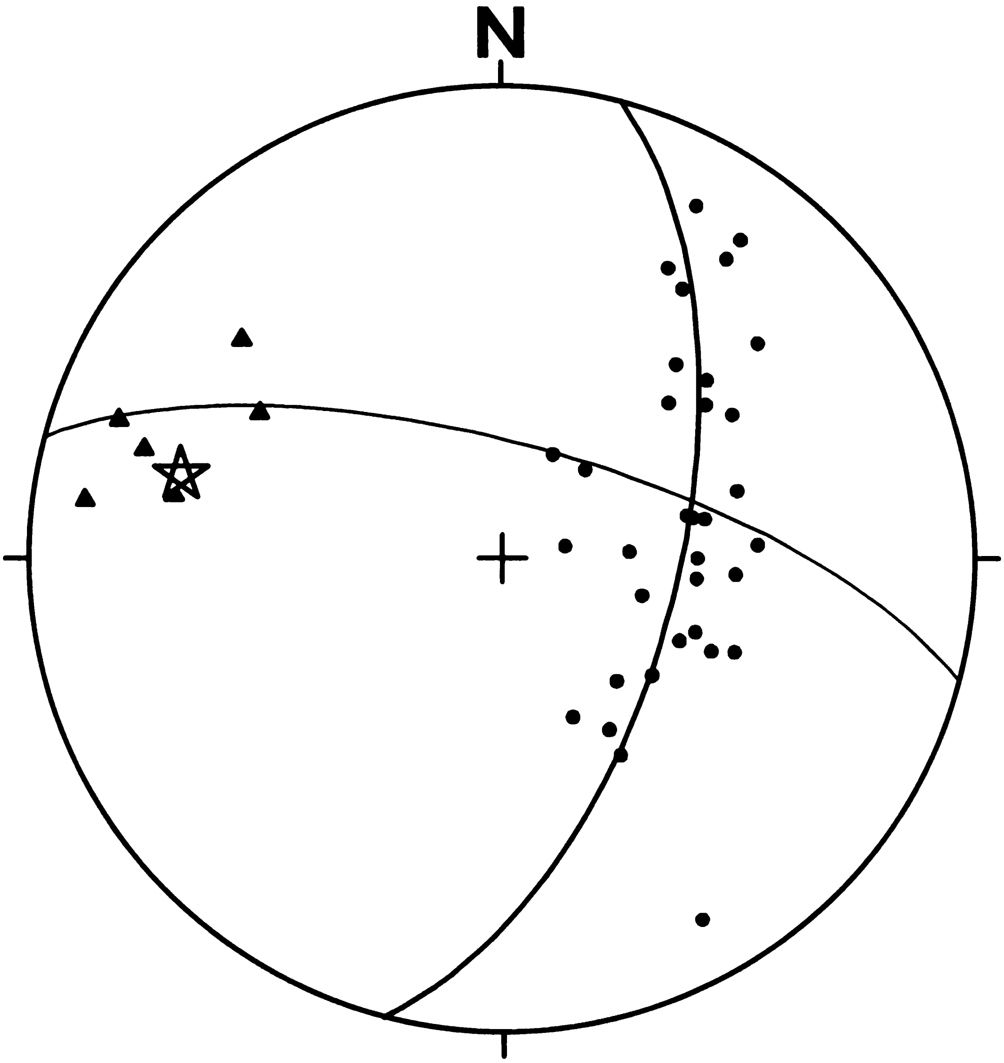

Figure 17. Stereonet plot of the 1710 bench on the Northeast wall of the Tilden Hematite pit. Fold axis (star) plunges towards the WNW as do the measured hinge lines (triangles). The poles to the bedding (circles) are distributed about a great circle (thick line), and the mean axial surface (thin line) dips to the NNE.

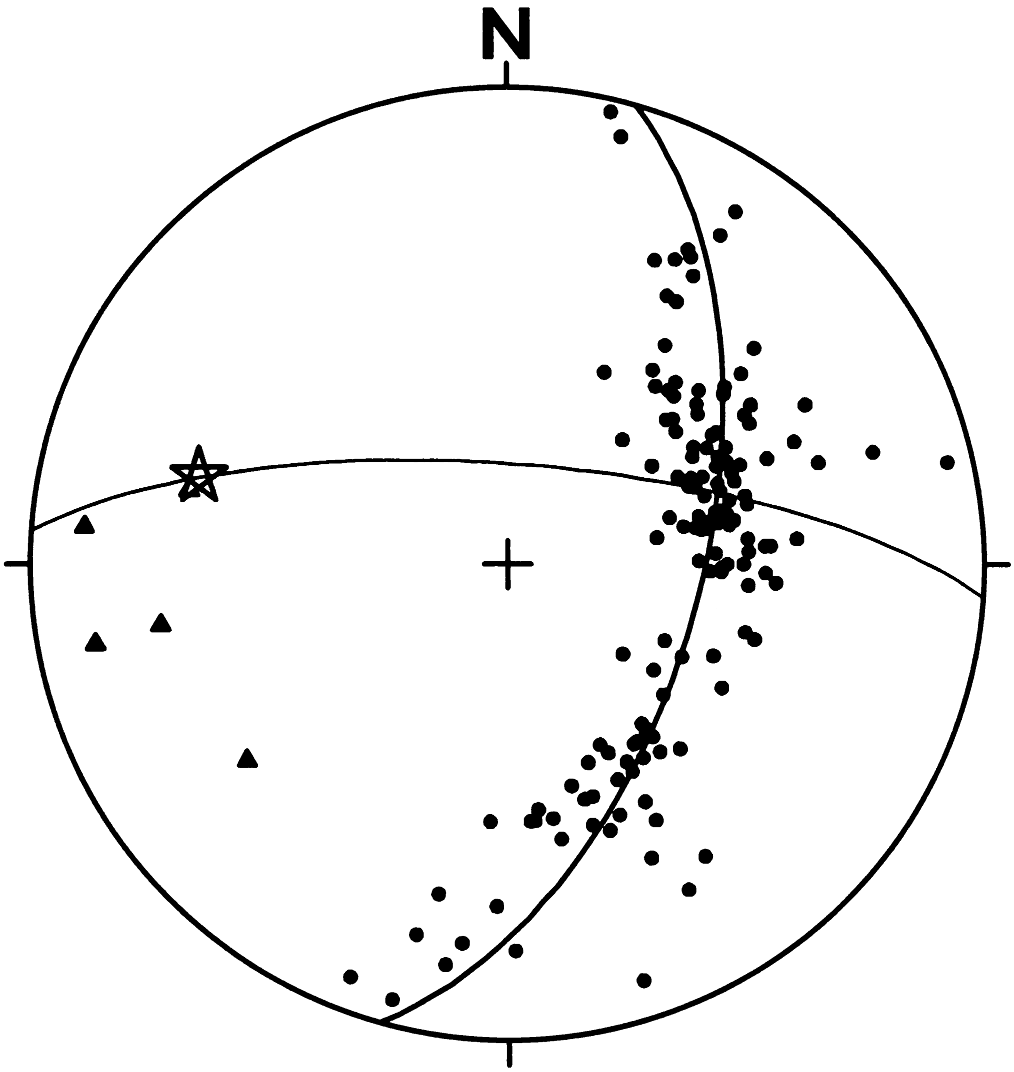

Figure 18. Stereonet plot of the anticline in the Empire Southwest Extension pit. The thick line represents the best fit great circle to the bedding poles (circles), the star is the fold axis, the triangles are the hinge lines, and the thin line represents the mean axial surface dipping to the NNE.

Main Pit

In the Main pit, two different folds were measured: one on the east side of the pit, labeled Fold One, and the other in the southeast corner, Fold Two. Fold One is exposed on the 1080 bench, and is an upright, symmetrically folded anticline that appears quite isolated. Fold Two is a large anticline with broad limbs; it is exposed throughout several benches but only measured on the 910 and 990 benches.

Fifty-two bedding planes on Fold One were measured as well as an approximation of hinge line and axial surface since no drag folds are present (Appendix A, Table 6). Bedding conforms to a great circle with a fold axis plunging to the NW at 30° (Figure 19). The axial surface is almost vertical but slightly dipping to the SW. This fold was deformed under a NE-SW compressive direction.

The geometry of Fold Two is similar to all the others. One hundred forty-one bedding planes straddle a great circle that gently plunges to the WNW (Figure 20). The mean axial surface dips to the NNE and the three measured hinge lines gently plunge 15° to the east. This fold was compressed from a NNE-SSW direction.

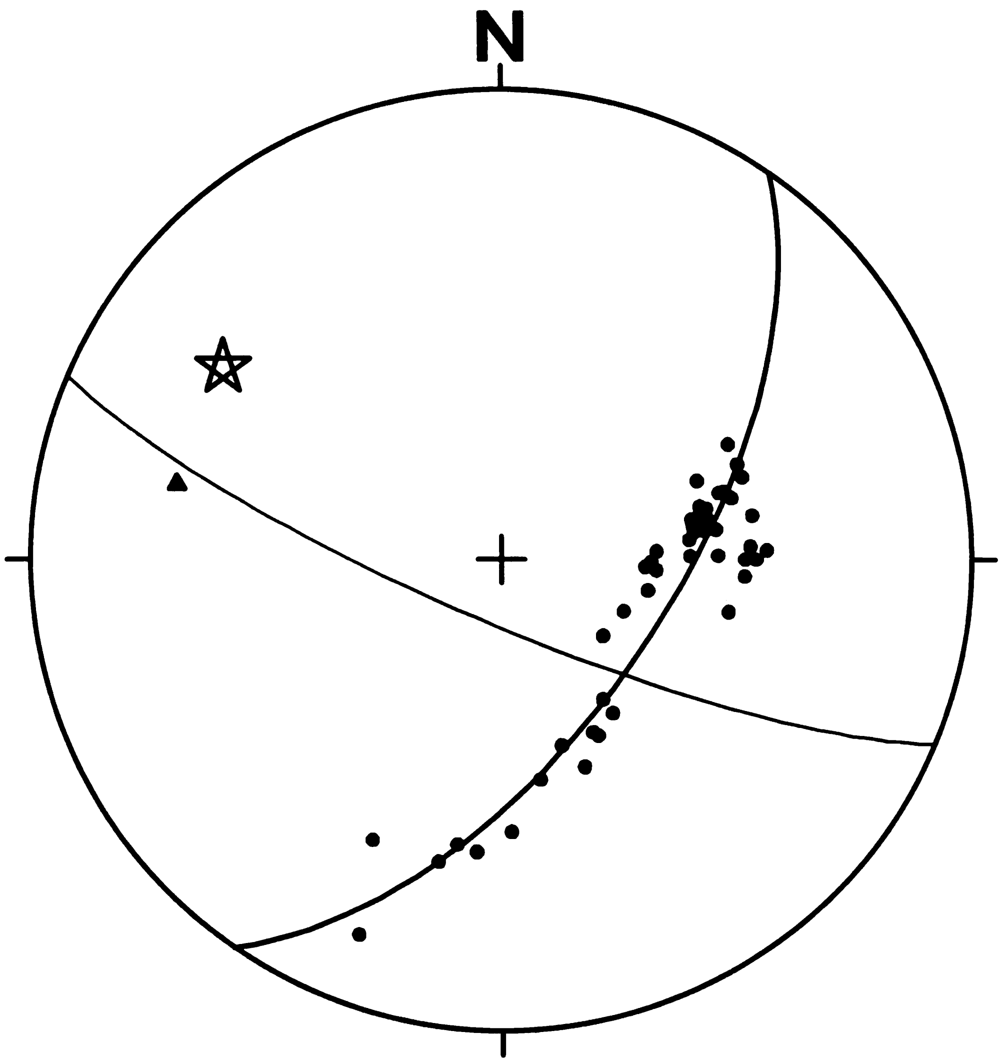

Figure 19. Stereonet plot of an anticline in Empire Main pit, labeled Fold One. The axial surface (thin line) dips to the SSW, hinge line (triangle) plunges to the WNW, the bedding poles (circles) conform to a great circle (thick line) with a fold axis (star) plunging to the NW.

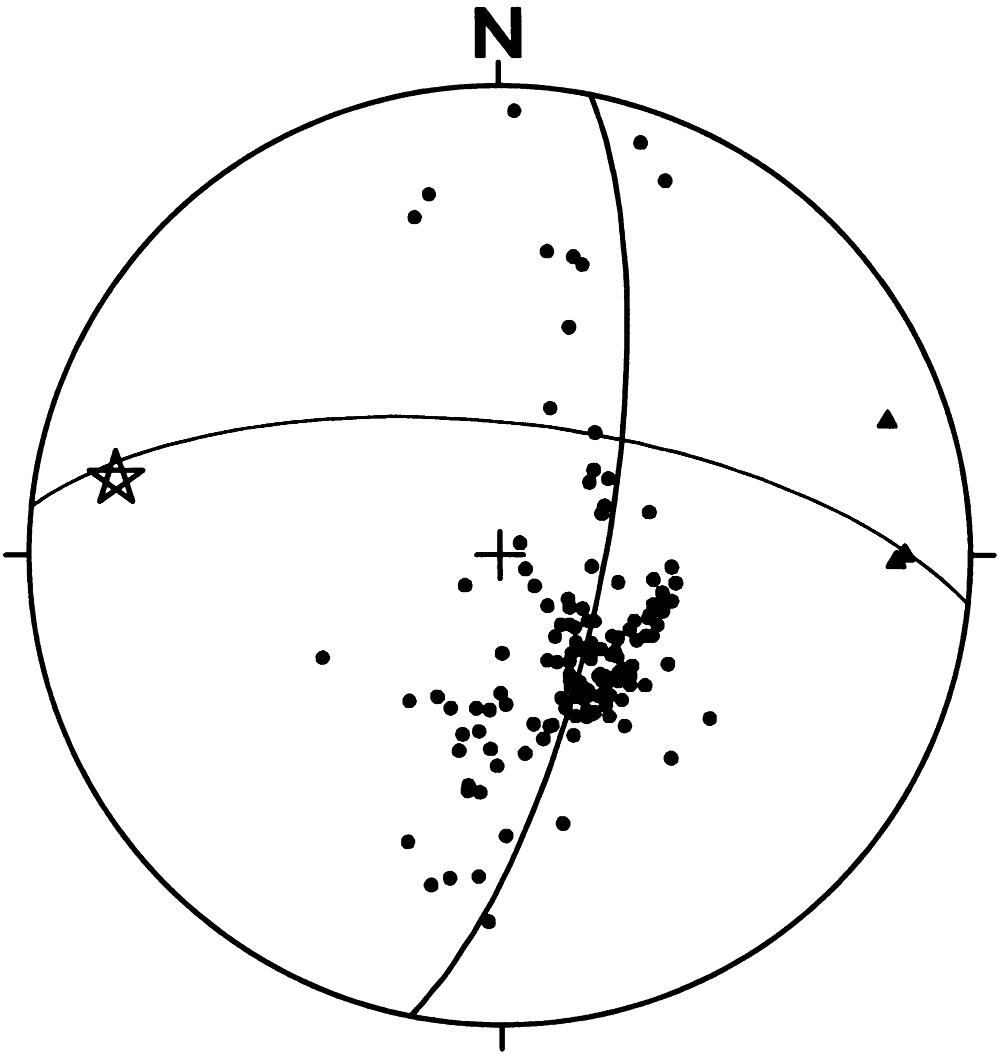

Figure 20. Stereonet plot of a fold in the Empire Main pit, named Fold Two. The fold axis plunges to the WNW and is represented by the star. Poles to bedding (circles) are distributed about a great circle (thick line). The hinge lines, represented by the triangles, plunge to the east. The axial surface, thin line, dips to the NNE.

TILDEN SHEAR ZONE PROTOLITH

Since 1895, the boundary between the Archean gneisses and the Early Proterozoic metasedimentary rocks, here described as a reverse ductile shear zone, has previously been interpreted as the altered equivalent of the lower Archean gneiss (Van Hise and Bayley, 1895). Gair and Simmons (1968) agreed with this early interpretation, however, they noted that the external characteristics of the Palmer Gneiss do not reveal the rock from which it was derived; i.e., it has a misleading name because it does not look like gneiss. They believed the PG was an example of retrograde metamorphism and offered three modes of genesis: (1) alteration and shearing of lower Archean gneiss during faulting, (2) migration of fluids along the contact between lower and middle Precambrian rocks, and (3) alteration of a regolith during folding. The recent Tilden Mine exposure of the PG and the presence of shear bands support Gair and Simmons (1968) first hypothesis for the rock formation. However, because of the characteristics of the PG, it is questionable whether the Archean gneiss, a dominantly granitic rock (Cannon and Simmons, 1973), is the protolith.

Several rock types are possible protoliths of the shear zone including the Southern Complex Gneiss, banded iron formation, a clastic lens, or a metadiabase sill. In an attempt to test and interpret the protolith of the PG, chemical analyses were conducted on several samples collected within the Tilden Mine area. From the analyses, the possibility of the banded iron formation as the protolith can be dismissed because of the lack of iron in the PG. No clastics are found in the PG suggesting that it did not form from the alteration of a clastic lens. The Southern Complex Gneiss, previously interpreted as the protolith, is a likely candidate because it is directly adjacent to the shear zone but is also discarded for reasons that will be discussed further on. However, it should be noted that the Southern Complex Gneiss abutting the PG is altered and shows a gradational contact into the shear zone. The metadiabase is here interpreted as the original rock of the PG, which suggests a Proterozoic, not an Archean age because the metadiabase intruded during the extensional stage in the Early Proterozoic. The sill is not adjacent to the shear zone, but it is a strong possibility because it may have been rotated into the shear zone during folding. Figure 21 shows a cross section through the Tilden Hematite pit interpreted from drill cores and bench maps; notice the anticlinal shape of the metadiabase (230), it appears that the southern limb may have been rotated into the footwall during shearing. With metadiabase as the protolith, the role of volume loss can be interpreted and then contrasted with a sheared dike of similar age and composition to the metadiabase sill within the Marquette trough.

Whole Rock Geochemistry

Samples were analyzed using X-ray fluorescence to determine the concentrations of major and trace elements. The samples included rocks mapped as PG (outside mine area), the sheared PG, gneisses of the Southern Complex, and metadiabase adjacent to the shear zone.

The sheared rock chemistry is indicative of a basaltic composition (Table 1). The gneissic rocks are much more silica rich and are slightly different from

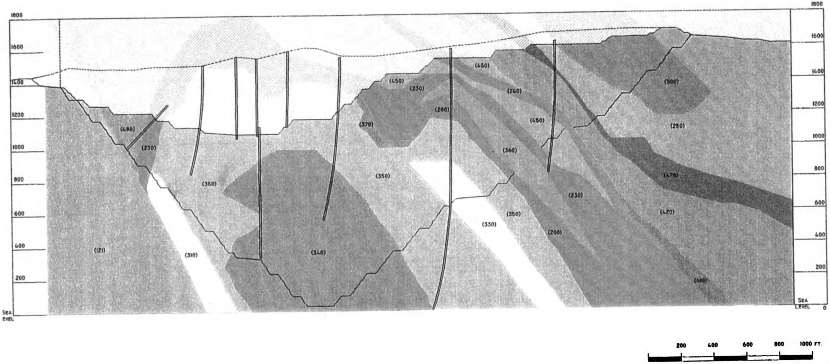

Figure 21. Diagrammatic cross section through the Tilden pit. Notice the metadiabase (230) sill is rotated next to the footwall shear zone. From Glenn and Lukey (1999).

Table 1. Mean chemical data for metadiabase, Palmer Gneiss, and Southern Complex Gneiss. Major oxides in weight percentage, trace elements in ppm. Line indicates element concentration below detection limit.

	Metadiabase (n = 7)	Palmer Gneiss (n = 14)	Southern Complex (n = 3)
ρ (g/cm^3)	2.85	3.03	2.73
SiO_2	49.83	51.83	73.15
TiO_2	2	1.09	0.19
Al_2O_3	14	15.88	15.37
Fe_2O_3	14.12	14.72	2.15
MnO	0.2	0.18	0.05
MgO	6.67	10.22	1.53
CaO	8.47	4.22	1.69
Na_2O	3.06	0.4	2.48
K_2O	1.45	1.66	3.35
P_2O_5	0.18	0.14	0.05
Ni	69.11	148.13	—
Zn	97.01	104.8	63.9
Rb	30.84	52.85	147.57
Sr	266.76	47.84	94.33
Y	16.14	27.22	27.97
Zr	98.93	85.51	72.7
Ba	1119.36	313.37	422.27

the sheared rock as seen on a plot of SiO_2 vs. other major oxides, in particular TiO_2, MgO, Fe_2O_3, and MnO (Figure 22). The sheared rocks are depleted in alkalis (Ca, Na) in comparison to either the metadiabase or the gneiss. Overall, the chemistry of the PG closely resembles that of the metadiabase (Figure 23). Thus, the major elements of the sheared rock are not consistent with a gneissic protolith, which suggests that the shear zone is an altered equivalent of the metadiabase.

Using the metadiabase as the protolith to the sheared rock, variations of the elements between the two are observed by the ratio of the average sheared rock/average protolith composition for major and trace elements (Figure 24). Nb and La were measured but were below detection limits for all samples. The PG is slightly enriched in SiO_2, Al_2O_3, Fe_2O_3, K_2O, Zn, Zr, and strongly enriched in MgO, Ni, Rb, and Y; whereas the PG is slightly depleted in MnO, P_2O_5, and strongly depleted in TiO_2, CaO, Na_2O, Sr, and Ba. Figure 24 gives an idea of the chemical changes that occurred. However, because the system was most likely open to fluids and elements with differing mobility, it gives only a vague insight on the transfer of components (Hippertt, 1998).

Volume Loss

During deformation of the PG, the rock changed both physically and chemically. Physically, the coarse-grained metadiabase, containing abundant feldspar, hornblende, and biotite, altered to well-foliated, fine-grained chloritic schist. Chemically, the rock changed resulting from elements moving in and out

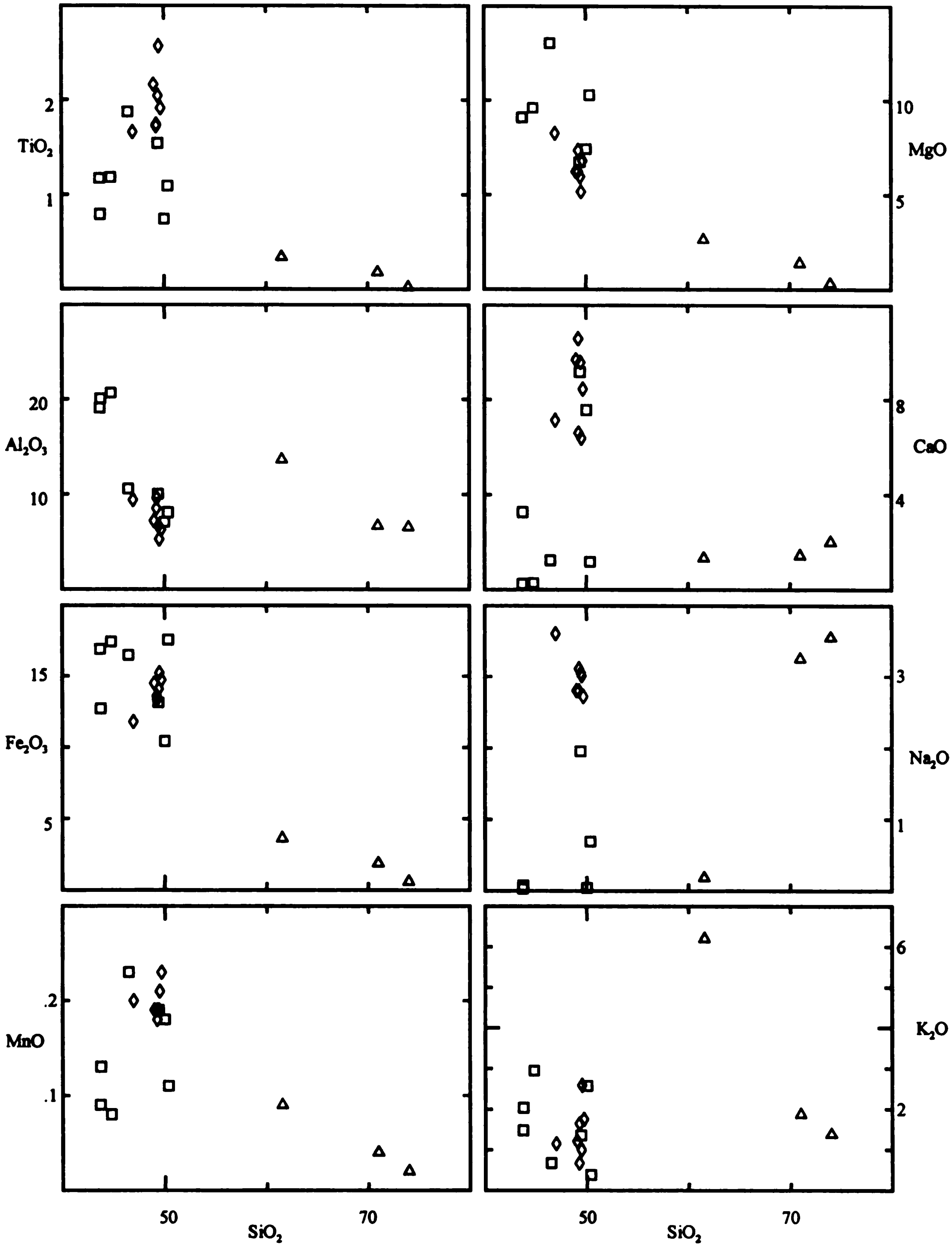

Figure 22. Plot of major oxides versus SiO_2 for all samples of metadiabase (diamond), Palmer Gneiss (square), and Southern Complex Gneiss (triangle).

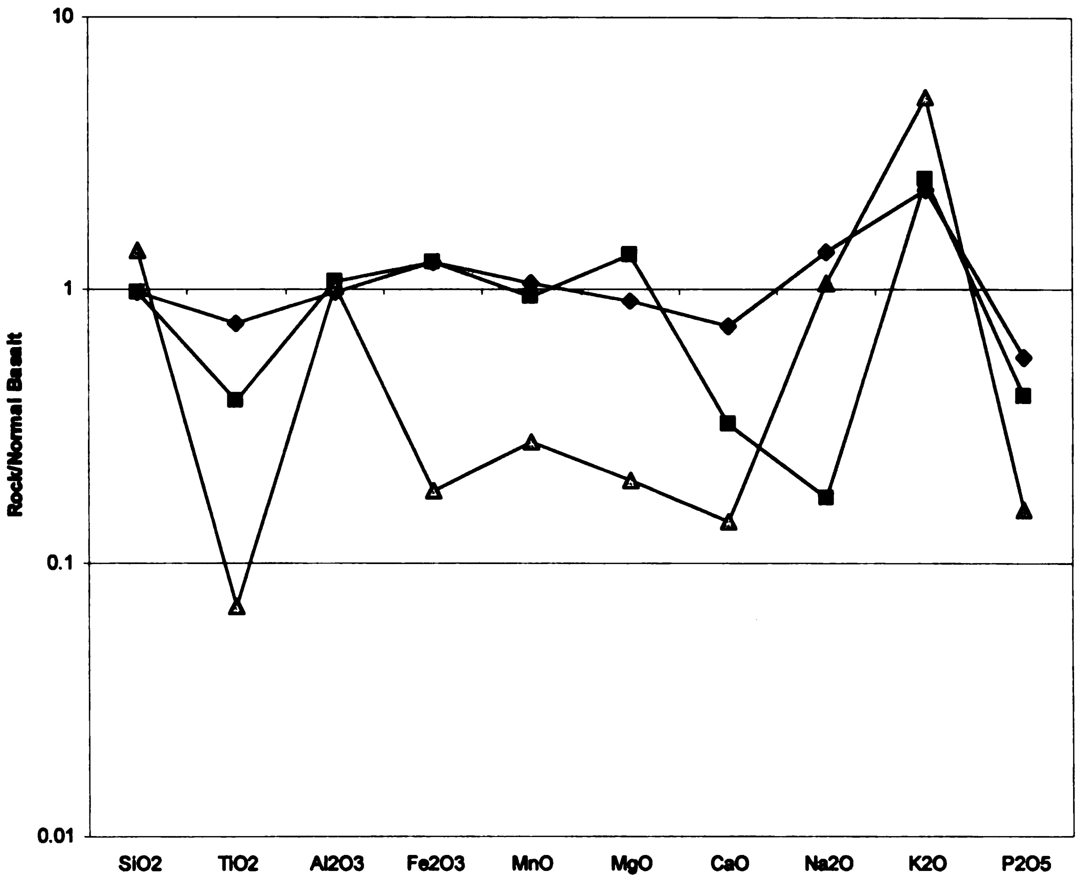

Figure 23. Comparison of major oxides concentrations of metadiabase (diamond), Palmer Gneiss (square), and Southern Complex Gneiss (triangle) plotted over a normal basalt composition.

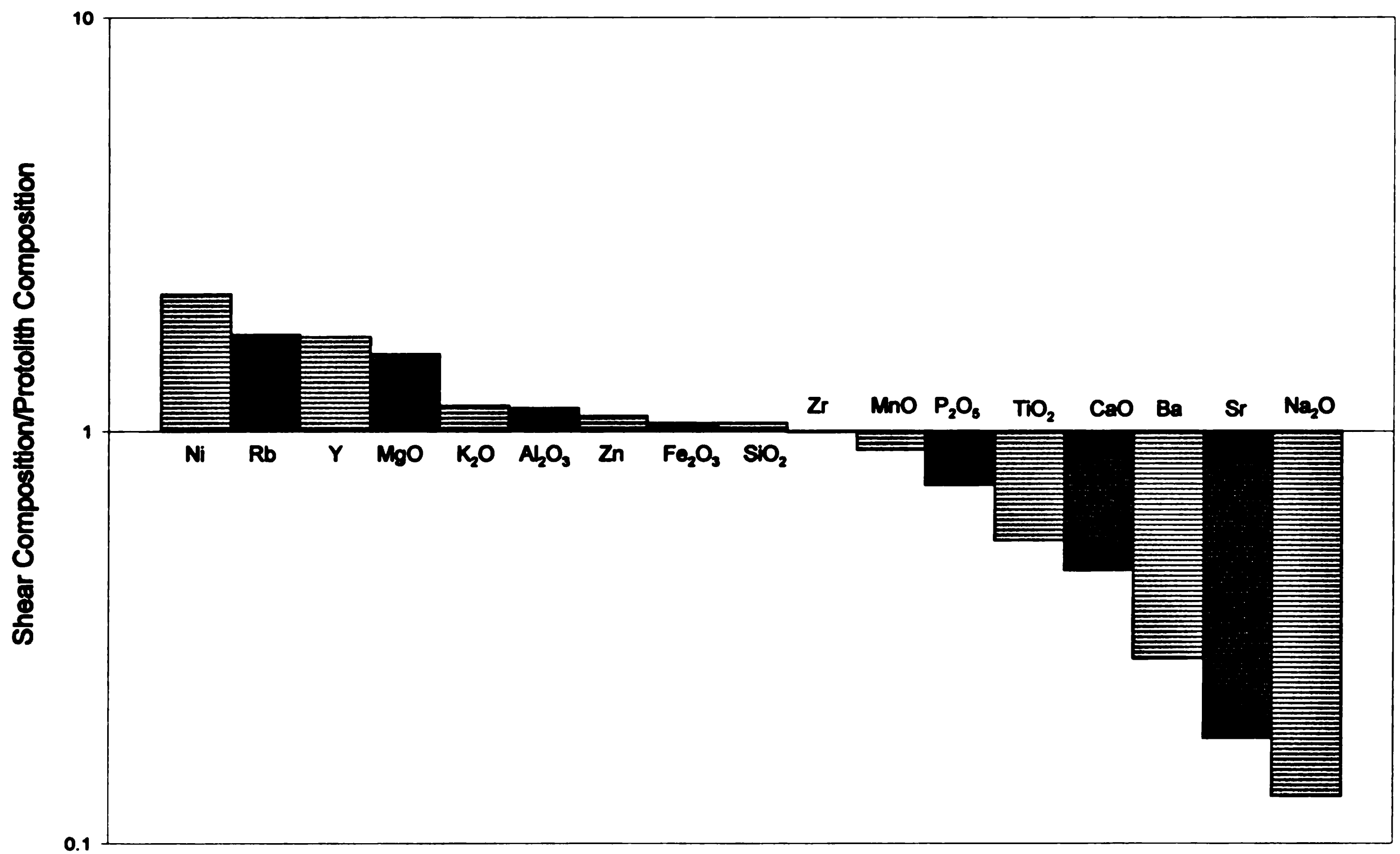

Figure 24. Ratio of average Palmer Gneiss, sheared rock, concentration versus the average metadiabase concentration on a logarithmic scale. Elements plotting above one are enriched in the sheared rock, values less than one are depleted in sheared rock.

of the system, a common effect shown in a number of mylonites (O'Hara, 1988; Glazner and Bartley, 1991; Hippertt, 1998; Ring, 1999). Dissolution and solution transfer are dominant processes that occur in shear zones with a large component of progressive shearing strain (Bell and Cuff, 1989) and under conditions of low metamorphic grade (Kerrich *et al.*, 1977). Elements of the minerals broken down and dissolved may be transferred out of the system resulting in a volume loss (Hippertt, 1998). Deformation involving volume loss is common in the upper crust (Bell and Cuff, 1989), and is an effective way of accommodating the strain (Ramsey and Wood, 1973).

Given the bulk chemical compositions of sheared rock and the protolith, further interpretations about the behavior of the elements and the amount of volume loss of the system can be explored. The volume relationship can be determined in two ways; Gresens' (1967) composition-volume relationship, and Grant's (1986) graphical solution to Gresens' method. Gresens' method is a mass balance equation that makes use of the bulk chemical analysis and the densities of the rocks involved in the metasomatism. According to Gresens' (1967), some components are likely to be immobile during alteration, and once these components are recognized, they are used to calculate the total amount of volume change. This assumes that the volume change is common to the behavior of all components, and assuming a chemically homogenous protolith. The basic equation behind Gresens' method is:

$$X_n = [f_v(g^B/g^A)C_n^B - C_n^A]100$$

where X_n is the amount of mass of a component that is either lost (negative value) or gained (positive value) in the system relative to the reference (immobile) component; f_v is known as the volume factor; g refers to the density of the rock; C represents the concentration of the component; and the superscripts A and B refer to the protolith and altered rocks, respectively. The value 100 refers to the reference mass of the original sample used for analyses that are summed to 100 weight percent. Within this equation, X_n and f_v are two unknown variables. If we assume that some of the components are immobile, assume a value for f_v, than it is possible to solve for the other variable, X_n.

To determine the immobile elements, a series of composition-volume equations are solved by rearranging the above equation to find the appropriate volume factor. Using the average compositions of metadiabase protolith and sheared rock adjusted to 100% (since all the analyses resulted in low totals), and densities of 2.85 g/cm^3 and 3.03 g/cm^3 for protolith and altered rock respectively, the composition-volume equations are as follows:

$f_v = 0.0181x_{SiO_2} + 0.9041$

$f_v = 0.8709x_{TiO_2} + 1.742$

$f_v = 0.0592x_{Al_2O_3} + 0.8298$

$f_v = 0.0640x_{Fe_2O_3} + 0.9028$

$f_v = 5.226x_{MnO} + 1.045$

$f_v = 0.0919x_{MgO} + 0.6142$

$f_v = 0.2783x_{CaO} + 2.354$

$f_v = 2.351x_{Na_2O} + 7.219$

$$f_v = 0.5632x_{K_2O} + 0.8167$$

$$f_v = 6.719x_{P_2O_5} + 1.277$$

These equations represent lines that all cross the zero gain-loss line (x-axis; Figure 25). The components that cross the x-axis furthest from one represent the highly mobile elements, while a tight clustering in the mid-portion of the graph indicates the immobile elements or the appropriate f_v value (Gresens, 1967). If $f_v = 1$, no volumetric change occurred during alteration; if $f_v < 1$, there was a net volume loss, and if $f_v > 1$, the volume increased. Note that Al_2O_3 and K_2O both cross the x-axis at a f_v value of 0.8298 and 0.8167, respectively, suggesting these are the immobile elements and an appropriate f_v value of 0.823. Inputing the f_v into the previous equations gives values for each oxide and results in the following mass balance equation that relates the chemistry of the sheared PG to the metadiabase:

$$\begin{aligned}&100\text{g protolith} + 4.48\text{g } SiO_2 + 2.27\text{g } MgO + 0.01\text{g } K_2O \longrightarrow\\ &87.5\text{g altered rock} + 1.06\text{g } TiO_2 + 0.11\text{g } Al_2O_3 + 1.25\text{g } Fe_2O_3 + 0.04\text{g } MnO\\ &+ 5.5\text{g } CaO + 2.72\text{g } Na_2O + 0.07\text{g } P_2O_5\end{aligned}$$

This equation shows that altering the metadiabase to the shear zone rocks resulted in an increase in SiO_2 and MgO, a loss in CaO and Na_2O, and an overall mass decrease of 12.5%. The volume factor subtracted from one suggests a volume loss of 17.7%.

The above result seems possible because Al is a low solubility element under many geologic conditions, and is often considered immobile. The Al in the plagioclase, hornblende, and biotite remained in the system and became

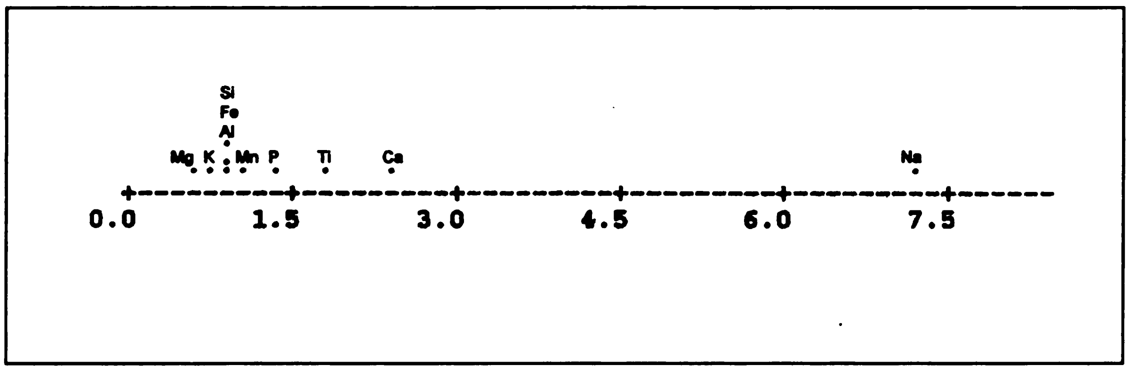

Figure 25. Plot of intersections of composition-volume equations with the gain-loss line of Gresens (1967). Note the tight clustering of potassium and aluminum oxides (fv = 0.823) and silica and iron oxides (fv = 0.903).

incorporated in the abundant chlorite. Using Gresens' method has severe limitations; in particular, Gresens example of choosing the appropriate f_v value was to develop a graph, such as Figure 25, and to find the immobile elements clustering somewhere in the central portion of the graph crossing the x-axis. This is quite arbitrary and can result in significant error; e.g., SiO_2 and Fe_2O_3 also cluster close together at a higher f_v value of 0.903, and this would result in a 4% decrease in mass with a 9.7% decrease in volume. The choosing of the f_v value is important and should be based on petrological reasoning. The errors introduced during XRF analysis and density estimates, as well as assuming a f_v value limits the computation of absolute values for volume loss.

The second method, Grant's (1986) graphical solution to Gresens' equation, was applied to the same compositional values of protolith and altered rock. The method is to plot the concentration of the altered rock (C_a) vs. the concentration of the protolith (C_o). An isocon, a line representing equal geochemical concentration, is drawn by inspection. The isocon is a best-fit line from the origin through a few points, which represents the immobile elements. The best-fit line through the data (Figure 26) suggests that both Al and K are immobile. The slope of the isocon, 1.143, is the inverse of $f_v(g^B/g^A)$ from Gresens' (1967), thus results in the same volume loss, 17.7%.

Grant (1986) noted that the term 'immobile' could be interpreted to mean two different things. First, it could mean that the component has undergone minimal mass transfer; or second, the concentration of a component has not changed in relation to another. Given this interpretation of the term 'immobile', Al

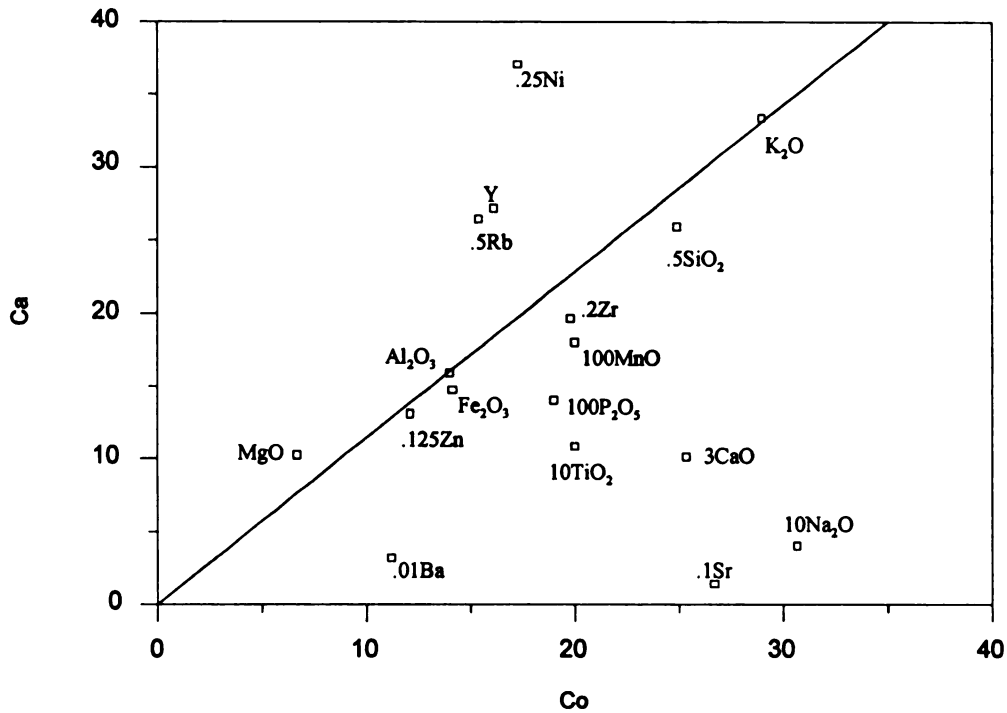

Figure 26. Isocon graph, concentration of elements in altered (Ca) rock versus concentration of elements in protolith (Co). The line (slope = 1.143) represents the isocon, equal chemical concentration.

and K can be used to define the isocon and be helpful in evaluating the behavior of the other elements during alteration. In Figure 27, the compositions or behavior of elements are compared to a constant mass isocon drawn from the origin through the protolith composition. Elements plotting above the line are gained by the system, and elements below the line are lost. Magnesium is the only element gained by the system, whereas all the other oxides are lost with respect to Al.

Republic Dike Comparison

Adjacent to the Marquette Synclinorium, in the Republic area, many mafic dikes cut into the Archean gneiss. These dikes were sheared during the Penokean Orogeny and exhibit sigmoidal shaped foliation patterns indicating the sense of motion (Myers, 1984). The margins of the dikes are highly strained and altered, while the center portions exhibit the least amount of strain and alteration. Michael Zieg (unpublished data) studied one of these dikes and conducted a chemical analysis across it (Table 2). Because the protolith of the dike is constrained, and similar to the metadiabase in the Tilden, it is beneficial to compare this sheared dike to the Tilden shear zone.

Both Gresens' (1967) and Grant's (1986) methods were applied to the data in the same manner as the Tilden shear zone to compare the element behavior and volume relationships. The center of the dike was used as the protolith and the margin was used as the altered equivalent. Figure 28 shows the variation of elements from the ratio of sheared concentration/protolith

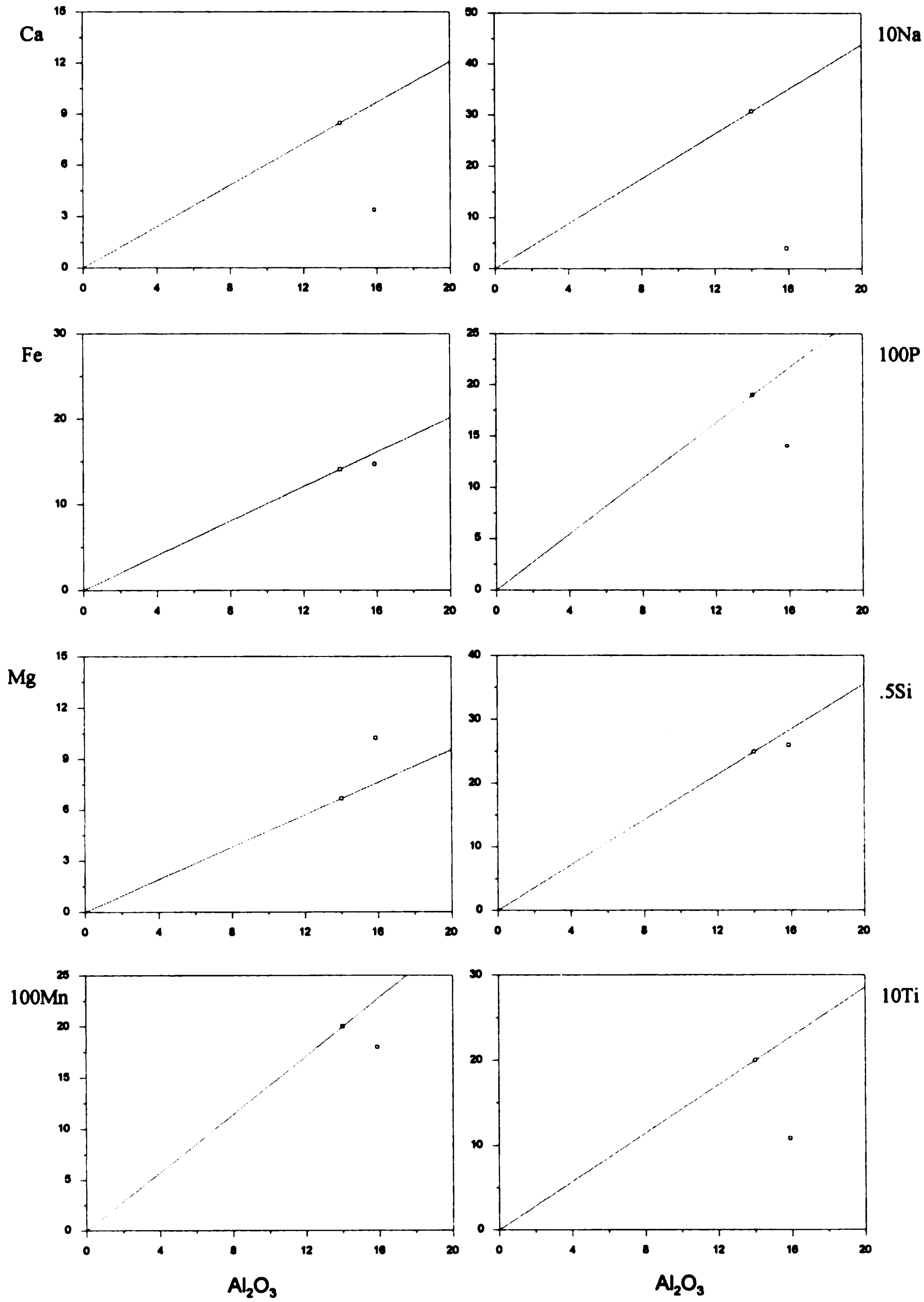

Figure 27. Plot of Al_2O_3 versus other major oxides. Line represents constant mass isocon. Elements above the line were gained by the system, elements below the line were lost with respect to Al_2O_3

Table 2. XRF whole rock major oxides of Republic dike, values are weight percentages (Zieg, unpublished data).

	margin	center
ρ (g/cm^3)	2.5	2.1
SiO_2	53.4	53.05
TiO_2	0.63	0.71
Al_2O_3	13.66	12.62
Fe_2O_3	9.41	10.24
MnO	0.13	0.17
MgO	9.21	9.15
CaO	4.53	8.66
Na_2O	2.13	1.88
K_2O	3.76	1.4
P_2O_5	0.05	0.07
totals	96.91	97.95

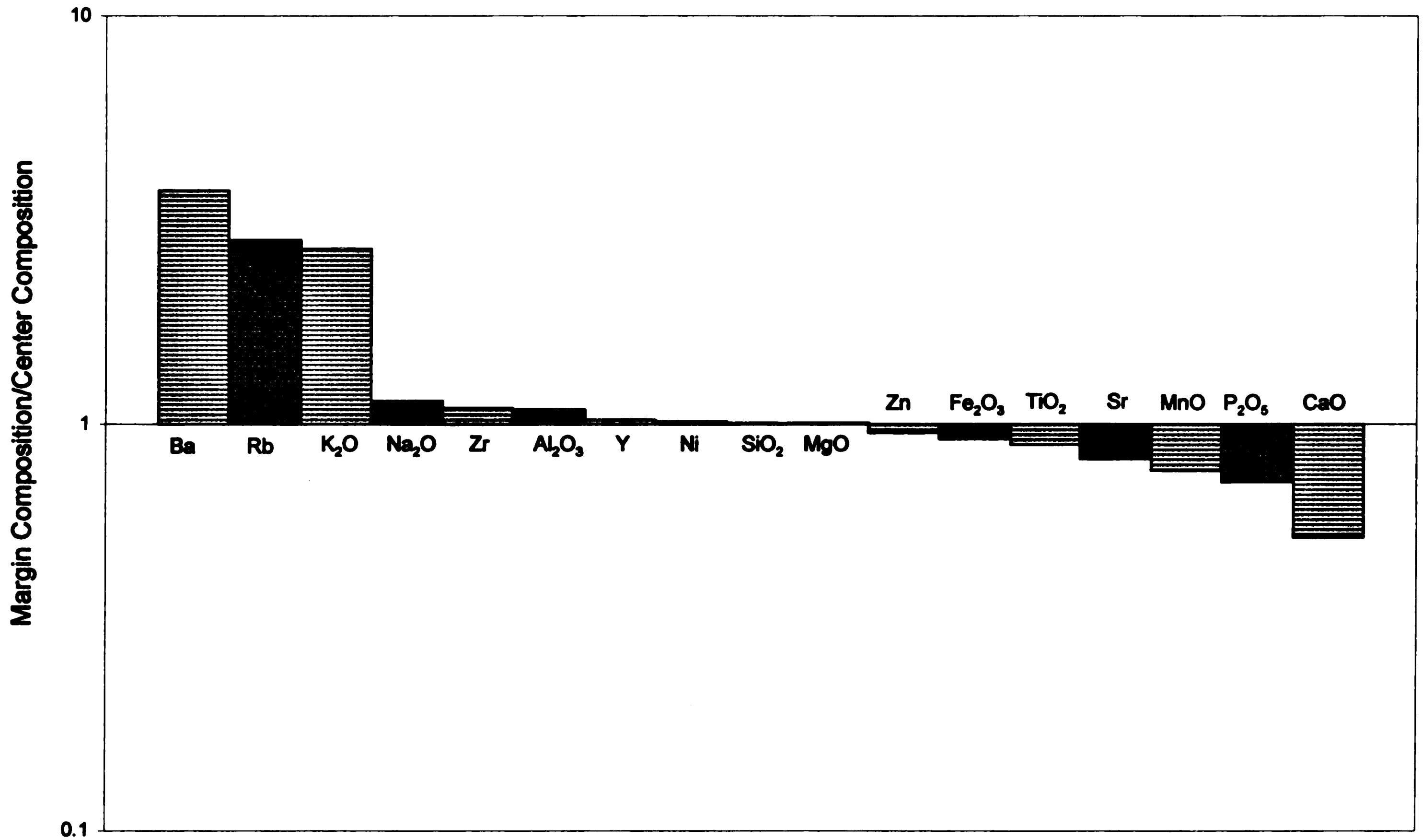

Figure 28. Ratio plot of the dike margin, or sheared rock concentration versus the dike center, or protolith concentration of a Republic dike on a logarithmic scale. Elements plotting above one are enriched in the sheared rock, values less than one are depleted in sheared rock.

concentration. Slightly enriched in the margins of the dike are SiO_2, Al_2O_3, MgO, Na_2O, Ni, Y, Zr and components strongly enriched are K_2O, Rb, and Ba. The margins are depleted in TiO_2, Fe_2O_3, MnO, CaO, P_2O_5, Zn, and Sr. The element variation of the dike is not much different than the Tilden shear zone (Figure 24); the major exceptions are Fe_2O_3, Zn, Na_2O, and Ba. Fe_2O_3 and Zn are enriched in the Tilden shear zone and depleted in the dike, while Na_2O and Ba are strongly depleted in the Tilden zone but slightly to strongly enriched in the dike.

To determine the amount of volume and mass change of the dike, Gresens (1967) composition-volume equations are as follows:

$f_v = 0.0152x_{SiO_2} + 0.8263$

$f_v = 1.292x_{TiO_2} + 0.933$

$f_v = 0.0596x_{Al_2O_3} + 0.7679$

$f_v = 0.0865x_{Fe_2O_3} + 0.9049$

$f_v = 6.269x_{MnO} + 1.075$

$f_v = 0.088x_{MgO} + 0.8259$

$f_v = 0.1799x_{CaO} + 1.59$

$f_v = 0.3822x_{Na_2O} + 0.7338$

$f_v = 0.2165x_{K_2O} + 0.3094$

$f_v = 16.28x_{P_2O_5} + 1.081$

Figure 29 shows a plot of the value of the X-intercepts upon crossing the zero gain-loss line when $X_n = 0$, suggesting Si and Mg are the immobile elements and indicate a f_v value of 0.826. This f_v value leads to the following balanced alteration equation:

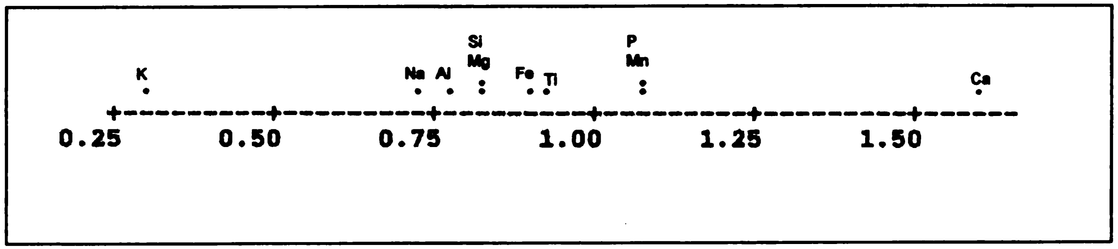

Figure 29. Plot of intersections of composition-volume equations with the gain-loss zero line (x-axis) of Republic dike alteration. Oxides of silica and magnesium are tightly clustered together at fv = 0.826.

$$100g\ protolith + 0.97g\ Al_2O_3 + 0.24g\ Na_2O + 2.39g\ K_2O \longrightarrow$$

$$98.3g\ altered\ rock + 0.02g\ SiO_2 + 0.08g\ TiO_2 + 0.91g\ Fe_2O_3 + 0.04g\ MnO + 4.25g\ CaO + 0.02g\ P_2O_5$$

Alteration of the dikes resulted in a 1.7% decrease in mass, and a 17.4% decrease in volume. The slope of a best-fit isocon is 1.017, suggesting Si, Mg, and Ni are immobile, however, many of the other elements plot close to the isocon, indicating not much mobility of those elements (Figure 30).

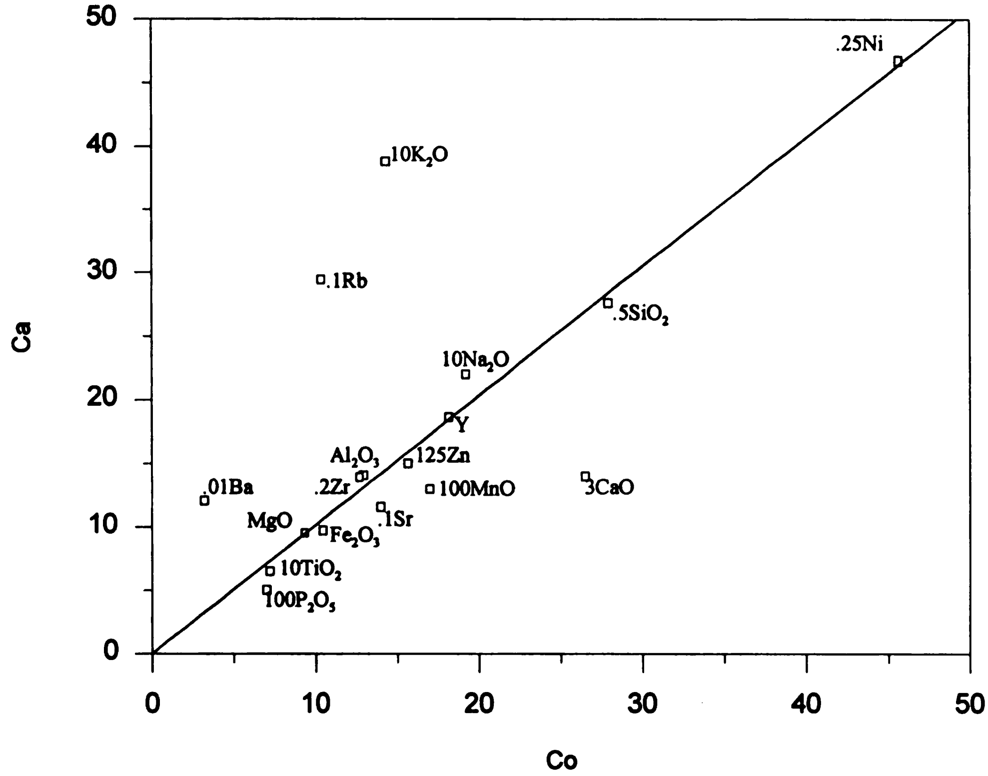

Figure 30. Isocon graph of Republic dike. Altered rock element concentration (Ca) versus element concentration of protolith (Co). Isocon has a slope of 1.017.

DISCUSSION

Deformation History

Structural analysis of the Tilden shear zone and folds within the Marquette Synclinorium indicate that they formed under a NNE-SSW principal shortening direction and are interpreted to have originated at the same time. The determination of the principle shortening direction confirm a previous study of sheared mafic dikes in the Republic area (Myers, 1984). Deformation is attributed to the Penokean Orogeny, when the region underwent compression due to an island arc colliding with the southern edge of the Superior Craton (Cambray, 1978). This major tectonic episode occurred 1.9-1.85 billion years ago (Van Schmus, 1976).

The Tilden shear zone is a large, reverse dip-slip ductile shear zone that contains mega-scale shear bands indicating a reverse sense of motion. The movement along this fault displaced the younger Early Proterozoic Marquette Range Supergroup up over the older Archean Gneisses. In order to thrust younger over older, the younger, MRSG, must originally have been stratigraphically lower i.e., deposited in a basin type setting within the Archean Craton. Much of the Lower MRSG is interpreted to have formed in a subsiding basin on a rifted passive margin (Larue, 1981; Larue and Sloss, 1980) or in a foreland basin (Barovich *et al.*, 1989). The pattern of younger over older is not restricted to the Tilden area, for it is also observed in the Harvey Quarry. The compressive direction of this shear zone is NNW-SSE, normal to the trough margin, similar to what Myers (1984) observed in his study.

The folds in the adjacent iron formation generally have a consistent geometry. The axes of the folds plunge to the WNW at approximately 30°. The axial surfaces dip steeply to the NNE. The orientations of these folds suggest that they were compressed in a NNE-SSW direction. One fold measured at the Empire Mine has a slightly different geometry, the fold axis is plunging more to the NW; this dissimilar geometry may possibly indicate a superimposed folding event as suggested from the complex folding seen at Jasper Knob.

The Marquette trough is an asymmetric basin, which lies adjacent to the Great Lakes tectonic zone of Sims et al. (1980). Evidence for the asymmetry of the basin is the truncated stratigraphy on the southern margin with a more complete succession on the northern side. The MT is similar to a classic rollover structure in a rift basin (Figure 31), and is supported by clastic lenses that are relatively thick in the south and fade out to the north (Breithart, 1983). During the development of the passive margin, the southern side of the trough was being uplifted, shedding sediments north into the basin; paleocurrents indicate a NE transport direction (Lin, 1969).

The end of sedimentation of the Early Proterozoic sediments is accredited to the progressive onset of the Penokean Orogeny. The compression caused closure of the basin and the reactivation of preexisting normal faults (Figure 32). The basin was inverted and resulted in a reverse dip slip along the southern margin of the trough. Inversion tectonics is a common phenomenon in Phanerozoic tectonics (Jackson, 1980; Gillcrist *et al.*, 1987; Chadwick, 1993). The strain was concentrated in a portion of a metadiabase sill that was rotated

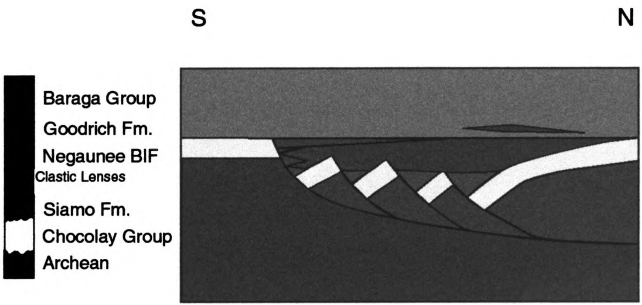

Figure 31. Schematic diagram of the pre-Penokean Marquette trough

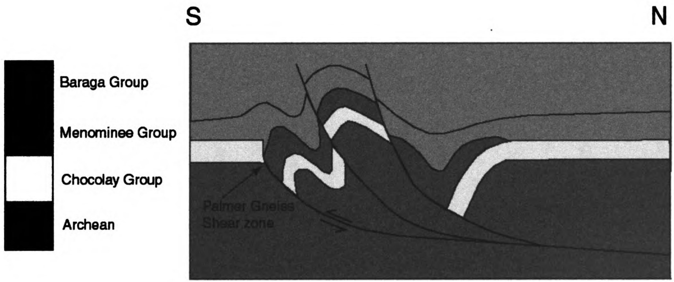

Figure 32. Schematic diagram of Marquette trough after Penokean deformation.

into the shear zone causing alteration and shearing of the rock to form the Palmer Gneiss.

Protolith and Mass-Volume Changes

The Tilden sheared rocks, PG, are interpreted to have been formed from the alteration of a metadiabase during shearing. Shear bands indicate ductile deformation during formation, and the "basaltic" type chemistry as well as external appearance of the sheared rock suggests that it did not form from the alteration of granitic gneiss as previously assumed. During metasomatic alteration, pressure solution and solution transfer can cause chemical modifications that may result in a mass and/or volume change (Kerrich *et al.*, 1977; Bell and Cuff, 1989). 'Some' bulk chemical changes may occur when rocks develop a foliation, and it is more likely in a rock with a higher phyllosilicate content (Bell and Cuff, 1989). The sheared PG rocks at the Tilden have a pronounced foliation and a high content of chlorite; the rocks have definitely undergone chemical changes when either of the two possible protoliths is considered. However, the chemical changes involved from the alteration of the gneiss to the sheared rocks seems too extreme, whereas the chemical changes form a metadiabase to sheared rocks is more probable.

The chemical modifications induced during deformation of the metadiabase are comparable to the chemical changes caused in a sheared Republic dike, which represents a known protolith that underwent shearing. The margins of the dike are altered relative to the central portion. The chemical changes from the margin to the center are similar to the changes form metadiabase (within trough) to the PG (Figures 24 and 28) indicating further evidence that the metadiabase is the protolith to the PG.

A compressional setting, which invokes shortening of the crust, was the tectonic framework that controlled the formation of the PG. Volume loss is a means of obtaining crustal shortening (Hippertt, 1998), and is interpreted to have occurred during alteration; calculations result in a 17.7% volume loss and a 12.5% decrease in mass. These changes in volume and mass are not absolute and are only approximations.

The approximations of changes were calculated using Gresens' (1967) composition-volume equations, and Grant's (1986) isocon method, a graphical solution to Gresens. The methods have many limitations that prevent the determination of absolute changes in volume or mass. The three main problems associated with the calculation of the volume and mass changes are (1) the potential for analytical error, (2) the assumption of homogeneous alteration, and (3) the choosing of the reference element(s). The problem of analytical error leads to uncertainties of chemical differences; analyzing several samples slightly minimized this problem. The second major problem is the assumption that the alteration was homogeneous. Alteration typically is concentrated along fractures and is commonly heterogeneous (Baumgartner and Olsen, 1995). The heterogeneity in the chemistry of the samples collected, i.e., the wide ranges in compositions among the altered rock samples (Appendix B) indicate that the alteration was not homogeneous. The problem of heterogeneity was not corrected for by the calculations used. The choosing of the appropriate reference element, the third problem, can cause the greatest source of error if the wrong element is chosen.

Low solubility elements such as, Ti, Al, and Zr are typically chosen as reference elements in many metasomatic alteration studies (O' Hara, 1988; Hippertt, 1998; Ring, 1999). Many geologic variables effect element mobility including the composition of the rock, pressure, temperature, and the presence of fluids (Ague and van Haren, 1996); thus, to assume one of those elements immobile for a given alteration may be unjustified because the conditions that controlled the mobility potential are not known or constrained. Therefore, no element can always be considered immobile, it is dependent upon the conditions, and additional information, such as petrographic evidence, is needed to make and support the appropriate choice of the reference element (Baumgartner and Olsen, 1995). Despite all the problems associated with the determination of volume and mass changes, the methods were used in an attempt to give a vague insight into the alteration of the PG.

CONCLUSION

The geometry of the large, low-grade shear zone exposed on the southern margin of the Marquette Synclinorium is that of reverse dip-slip. The mega-shear bands indicate a NNE-SSW compressive direction, confirming previous studies of sheared mafic dikes (Myers, 1984). The shear zone was produced when the Penokean Orogeny caused closure of the basin, and localized strain in part of the metadiabase sill that was rotated into the shear zone causing alteration and shearing to form the Palmer Gneiss.

The appearance and the chemistry of the PG suggest that it did not form from the alteration of gneiss as previously interpreted, but that it is an altered equivalent of metadiabase indicating a Proterozoic age. The chemical changes that occurred in forming the altered PG are comparable to the chemical changes in a sheared mafic dike of similar origin in the Republic area. Volume and mass loss accompanied the alteration. The best approximations of loss in the Tilden shear zone are 17.7% in volume and 12.5% in mass.

A geometrical relationship exists between the shear zone and the folds in the adjacent Negaunee Iron Formation. This suggests that the folds and the shear zone were produced at the same time under the same compressional conditions. The Marquette trough is a Precambrian example of inversion tectonics. Reactivation of preexisting faults has been noted in many studies in Phanerozoic settings. This suggests that the tectonics during the Precambrian were similar to the tectonics taking place today.

APPENDIX A

Table 1. Measurements of foliations in the Tilden footwall, south side of Hematite pit. Measurements are dip direction/dip amount.

Tilden Footwall							
S-foliation	(n = 253)					C'-foliation	(n = 77)
020/61	039/73	009/71	342/64	014/69	014/61	351/55	355/38
016/62	033/65	014/81	352/67	028/54	357/66	349/49	347/38
016/65	016/73	322/63	346/72	025/59	003/73	016/45	021/26
021/64	036/69	026/78	007/86	028/55	036/64	009/50	023/20
022/71	032/72	044/81	357/61	025/53	353/71	335/54	003/28
352/70	032/87	006/75	008/57	029/60	353/69	340/50	020/43
001/55	019/77	011/71	360/61	039/62	028/69	355/48	003/34
358/49	036/82	017/72	001/61	038/54	354/51	036/43	026/43
002/53	046/80	005/65	357/63	038/60	017/61	013/51	322/30
352/56	025/72	009/75	029/72	022/62	009/55	041/54	332/33
352/65	019/67	001/63	217/90	006/64	017/76	007/51	014/31
003/61	016/74	018/66	338/63	017/61	038/63	038/35	350/32
349/70	025/75	013/68	027/70	026/78	028/53	015/31	005/31
002/67	201/89	012/58	330/75	356/53	349/53	025/35	010/27
043/76	022/69	014/72	334/74	009/55	013/53	009/48	345/36
031/80	032/85	011/62	360/70	002/60	355/58	022/19	023/45
349/88	014/69	341/59	012/71	020/66	013/58	021/49	347/34
355/57	003/76	315/82	356/75	019/64	012/66	023/51	357/37
028/68	010/74	357/63	351/75	016/66	013/73	016/20	017/28
003/61	014/69	353/67	350/75	019/77	016/77	087/30	343/42
012/63	010/69	033/63	008/69	014/69	352/56	014/39	024/41
023/53	019/78	016/59	024/64	001/64	355/59	357/47	008/50
006/68	004/69	027/73	010/68	015/56	032/64	015/33	003/36
000/61	352/55	005/63	353/82	008/67	021/86	043/49	022/37
037/74	022/85	021/66	349/83	021/67	023/72	026/31	353/46
035/71	013/58	349/49	335/85	018/63	022/59	345/36	338/55
014/77	021/74	046/86	332/82	021/67	008/78	008/32	020/37
010/74	011/54	023/75	033/66	358/63	225/86	009/39	003/45
015/66	006/72	027/89	035/61	009/61	036/79	035/48	009/58
022/61	014/68	030/89	357/59	015/62	035/77	007/50	352/54
030/70	037/79	029/80	026/58	029/61	022/76	338/31	312/46
022/64	012/90	002/86	025/78	044/69	047/70	360/35	004/34
007/69	009/71	018/78	044/88	007/70	017/73	354/51	020/52
337/61	007/70	001/82	011/60	025/67	356/60	341/49	357/48
015/66	054/54	014/84	012/68	032/67	348/80	358/49	
032/70	341/57	027/74	028/58	009/66	037/65	003/56	
015/73	346/59	025/67	016/58	023/63	012/60	001/52	
018/67	353/75	021/89	008/67	012/68	027/57	008/52	
021/67	349/59	014/67	018/57	029/62		337/51	
037/89	010/75	026/74	025/54	020/63		002/41	
016/73	020/79	016/69	355/55	309/75		003/52	
017/67	027/84	022/71	028/52	018/60		348/40	
001/60	005/67	007/74	004/75	029/60		013/55	

Table 2. Measurements obtained in the Harvey Quarry, including bedding, S-foliations, and C'-foliations. Dip direction/dip amount.

Bedding			
(n = 27)			
355/41	042/32	005/40	165/77
356/41	019/48	023/26	164/54
358/51	013/45	173/79	164/69
335/47	015/31	156/52	165/56
015/40	010/30	185/87	163/61
012/39	050/12	186/86	160/65
006/37	054/32	170/79	
S-foliation		C'-foliation	
(n = 10)		(n = 8)	
354/72	340/80	015/40	015/18
330/81	355/82	016/41	015/26
344/77	330/84	011/35	024/30
342/88	353/81	020/35	
352/75	350/80	027/25	

Table 3. Data for benches 1440 and 1530 in the Tilden Hematite pit. Measurements are dip directions/dip amount of bedding, hinge lines, and axial surfaces.

Bench 1440							
bedding						hinge line	axial surface
(n = 138)						(n = 17)	(n = 22)
320/45	031/18	184/78	061/18	220/65	201/82	299/21	021/65
349/57	324/34	068/57	354/42	024/42	219/65	105/08	005/64
348/63	311/35	178/61	322/36	203/80	211/84	287/15	050/83
216/13	316/44	301/41	282/27	203/78	302/57	107/08	015/77
318/25	311/35	293/36	355/60	208/83	250/58	276/06	026/73
289/14	004/42	347/29	258/34	201/84	016/50	295/30	024/88
017/24	051/50	322/30	243/43	202/82	001/71	279/23	004/84
006/58	335/42	321/34	241/43	205/69	029/43	293/49	010/63
309/21	330/42	324/43	235/30	221/69	222/58	291/28	019/67
319/35	341/35	347/55	241/30	344/48	333/66	277/30	254/66
348/28	353/65	348/53	247/34	193/80	262/54	290/42	236/80
268/26	347/35	286/47	237/37	010/36	321/39	293/49	280/28
359/36	347/47	219/80	250/30	028/53	336/65	303/50	012/73
251/33	316/56	011/81	244/36	009/61	223/60	286/37	016/76
276/44	017/32	211/40	250/38	016/59	226/46	304/46	012/78
221/37	348/47	287/39	328/38	041/72	239/44	271/23	200/88
251/41	353/44	323/56	231/32	358/64	232/34	293/23	008/77
219/57	351/44	230/52	249/27	349/45	241/61		197/85
231/51	334/20	214/72	244/45	025/83	225/43		001/62
223/44	330/29	236/66	006/63	193/89	199/70		207/81
216/50	359/44	265/40	252/44	214/77	015/79		359/70
222/56	247/23	264/53	254/34	206/78	202/66		229/84
205/88	348/40	208/65	234/49	025/89	236/51		
Bench 1530							
bedding						hinge line	axial surface
(n = 17)						(n = 4)	(n = 4)
179/83	355/34	185/70	215/65	195/85	196/67	295/23	018/79
180/78	357/87	209/79	018/86	183/86	201/72	279/38	348/72
204/79	173/85	352/60	325/65	346/35		268/43	324/50
						281/32	035/85

Table 4. Data for bench 1710 on the northeast side of the Tilden Hematite pit. Measurement are dip direction/dip amount of bedding, hinge lines and axial surfaces.

Bench 1710					
bedding				hinge line	axial surface
(n = 35)				(n = 6)	(n = 3)
292/44	229/48	233/45	257/33	310/29	010/59
258/34	259/36	329/40	294/40	287/22	022/82
206/20	291/36	285/25	230/60	290/15	013/72
295/34	267/45	331/76	238/48	301/40	
223/21	274/41	267/22	317/29	278/12	
270/34	276/34	336/30	259/11	281/30	
254/43	227/40	336/30	222/46		
217/73	328/35	217/68	214/58		
210/60	308/33	209/74			

Table 5. Data for the Empire Southwest Extension pit. Measurements are dip directions/dip amount of bedding, hinge lines, and axial surfaces.

SW-Extension							
bedding						hinge line	axial surface
(n = 152)						(n = 5)	(n = 5)
342/43	321/42	269/33	238/43	274/47	240/49	259/13	335/76
333/35	321/38	257/37	258/31	266/45	260/39	233/32	042/89
325/41	342/48	260/35	223/29	266/46	243/41	260/27	003/78
350/45	336/48	270/38	308/25	271/37	245/42	275/12	004/83
349/49	340/43	286/43	296/30	259/40	245/35	283/32	358/46
344/40	324/38	256/38	256/37	256/43	251/36		
354/45	339/50	270/41	275/42	231/49	242/60		
002/61	333/42	259/37	272/45	252/58	238/49		
355/45	342/81	254/29	225/41	211/64	213/77		
334/58	330/52	272/37	287/45	193/87	238/38		
330/48	326/63	240/40	267/42	213/61	245/40		
338/37	325/38	260/34	265/51	237/51	253/69		
332/37	329/40	228/37	248/42	209/62	012/60		
353/43	298/34	236/30	267/42	256/34	009/74		
321/38	207/37	240/37	232/42	232/48	007/69		
359/70	320/36	254/43	257/34	223/41	004/45		
320/37	300/43	248/49	243/33	213/71	014/69		
329/42	294/39	250/42	230/43	229/58	021/82		
331/67	258/36	272/35	238/42	242/43	015/84		
306/31	246/37	267/36	247/34	229/38	232/37		
310/35	257/39	249/39	248/35	260/26	232/37		
195/82	259/33	223/41	259/35	247/55	228/45		
317/44	258/37	245/41	264/42	247/44			
320/39	258/37	251/39	254/40	257/84			
210/65	206/60	213/55	231/53	223/43			
216/47	209/62	211/55	220/40	217/42			

Table 6. Data for Fold One and Two in the Empire Main Pit. Measurements are of bedding, hinge lines and axial surfaces as dip direction/dip amount.

Fold One							
bedding						hinge line	axial surface
(n = 52)						(n = 1)	(n = 2)
261/36	243/45	342/34	265/39	025/55	258/34	283/30	214/72
259/34	251/45	338/39	258/35	021/74	256/36		192/86
262/34	260/45	012/55	283/41	268/47	262/36		
259/37	255/36	350/39	267/44	262/38	248/37		
260/34	264/33	009/51	274/43	269/38	274/27		
269/33	271/26	358/48	270/45	259/35	273/25		
293/23	267/27	005/52	270/43	256/37	324/33		
257/36	282/26	307/22	324/30	253/41			
331/35	248/45	332/34	253/40	255/42			
Fold Two							
bedding						hinge line	axial surface
(n = 141)						(n = 3)	(n = 10)
287/29	319/29	312/26	336/28	194/55	002/67	091/17	016/70
294/30	325/30	296/26	326/34	303/14	003/34	090/15	010/75
289/30	313/31	300/26	332/32	315/17	004/27	071/14	358/71
292/28	302/28	308/47	330/32	317/23	004/58		342/67
288/28	298/30	314/29	330/29	005/42	008/41		354/62
293/28	306/25	323/30	349/30	231/20	009/27		359/63
283/29	313/29	317/30	338/34	012/61	018/28		357/66
285/31	310/30	328/26	319/20	314/22	024/27		028/77
279/27	320/33	325/32	312/08	007/31	032/30		023/67
279/31	329/32	306/24	166/63	347/49	049/08		012/63
274/30	315/32	313/24	337/27	235/23	060/36		
322/31	319/28	321/28	321/27	018/54	169/67		
299/29	303/35	331/31	305/25	001/37	182/84		
310/26	313/29	327/29	204/76	320/47	189/55		
319/22	317/12	283/21	228/22	299/05	196/54		
239/04	314/18	305/20	199/27	012/32	199/82		
336/20	307/15	326/17	218/27	245/20	254/27		
337/29	335/31	324/21	332/26	317/22	332/28		
197/42	303/17	332/21	327/22	359/17	344/31		
343/31	307/19	320/21	320/27	347/33	353/35		
331/25	330/25	319/16	277/16	324/37	358/26		
319/29	319/24	317/30	009/59	012/35	360/24		
322/21	327/28	248/19	312/34	359/50			
330/24	328/27	315/29	311/27	008/42			

APPENDIX B

Table 1. XRF whole rock chemical data for major oxides and trace elements of Palmer Gneiss, metadiabase, and Southern Complex Gneiss.

	Palmer Gneiss														Metadiabase							Southern Complex gneiss		
Sample	14	17	18	19	20	21	23	28	29	30	31	32	33	34	8	42	43	44	45	46	47	25	26	27
SiO_2	44.82	50.06	43.75	50.4	43.78	46.51	49.43	49.98	47.07	44.58	60.87	53.81	47.18	49.4	49.54	49.7	49.04	49.29	49.46	49.27	46.97	61.56	74.01	71
TiO_2	1.18	0.74	1.17	1.09	0.79	1.87	1.54	0.78	0.71	0.77	0.47	0.88	0.72	1.56	2.57	1.91	2.16	1.74	2.04	1.72	1.66	0.34	0.02	0.18
Al_2O_3	20.32	13.53	19.52	14.03	20.03	15.28	15.01	14.36	12.06	15.48	7.88	13.83	14.99	12.59	12.64	13.14	13.59	14.8	13.33	14.25	14.7	16.81	13.27	13.34
Fe_2O_3	17.43	10.41	16.91	17.58	12.7	16.48	13.13	12.41	10.34	14.98	9.1	14.89	11.67	15.63	15.24	14.74	14.48	13.35	14.09	13.59	11.78	3.62	0.58	1.86
MnO	0.08	0.18	0.09	0.11	0.13	0.23	0.19	0.17	0.25	0.21	0.28	0.1	0.2	0.15	0.21	0.23	0.19	0.18	0.19	0.19	0.2	0.09	0.02	0.04
MgO	9.58	7.41	9.06	10.26	9.06	13.02	6.72	11.21	10.2	13.72	9.34	7.25	9.07	8.51	5.16	6.79	6.23	7.34	5.94	6.23	8.24	2.63	0.3	1.38
CaO	0.28	7.55	0.24	1.17	3.26	1.23	9.17	2.02	8.75	2.27	4.54	2.02	4.57	3.8	6.37	8.45	9.69	6.58	9.58	10.58	7.12	1.33	2	1.43
Na_2O	0	0.04	0.03	0.69	0.07	0	1.95	0.6	0.92	0	0	0.01	0.03	1.02	3.01	2.72	2.8	3.11	3.05	2.8	3.61	0.18	3.55	3.25
K_2O	2.94	2.57	1.48	0.38	2.03	0.67	1.35	1.92	1.12	1.24	0.68	2.09	3.11	0.27	2.59	1.75	1.21	1.64	1	0.67	1.15	6.2	1.38	1.87
P_2O_5	0.19	0.09	0.16	0.18	0.09	0.22	0.18	0.08	0.08	0.08	0.05	0.09	0.08	0.25	0.25	0.16	0.18	0.16	0.19	0.15	0.19	0.1	0.01	0.05
totals	96.81	92.58	92.43	95.89	91.94	95.51	98.67	93.53	91.5	93.33	93.21	94.97	91.62	93.18	97.58	99.59	99.57	98.19	98.87	99.45	95.62	92.86	95.14	94.4
Cr	0	256.6	1710.2	64.1	263.3	157.1	158.2	310	276	337	163	343	331	96	0	78.8	112	256.4	97.7	214	1067.7	10.6	0	3.6
Ni	102.4	135.3	312.7	64.6	346.7	99.4	107.5	178.9	155.4	178.8	79.5	140.9	118.4	53.3	25.4	36.5	33.7	72.8	31.6	49.9	233.9	6.2	0	-14
Cu	11.6	218.8	22.9	101.3	3.1	4.5	85.5	270.4	20.3	1	27.4	16.9	24.5	75	84.8	100.1	201.8	39.8	162.5	57.4	157.2	20.2	18.6	62.4
Zn	122.1	69.7	127.3	135.4	153	94.9	92.3	103.9	75.2	125.8	82	94.9	73.9	116.8	105.9	107.8	100.7	89.7	86.6	90	98.4	68.5	14.5	108.7
Rb	85.4	72.8	83.8	6	130.3	13.5	32.1	52.4	21	51.4	32.3	56.8	91.5	10.6	55.9	43.1	32.7	29.7	20	11.7	22.8	312.9	50.7	79.1
Sr	1.1	39.9	0	0.4	31.6	3.5	432.5	18.8	60.4	6.8	23.2	8.1	15.3	28.1	198.2	284.4	313.8	284.8	250.4	344.5	191.2	15.3	113.3	154.4
Y	38.6	21.9	24.9	49.4	13.3	18.4	20.5	10.9	28.8	26.7	12	47.3	14.2	54.2	19.5	15.7	16.8	16.2	18	14.8	12	33	29.3	21.6
Zr	177.1	44.5	169.6	228.1	46.4	142.3	126.3	39.9	41.3	39.1	25.3	44.2	39.4	210.8	122.5	91.8	101.9	91	97.3	100.7	87.3	93.4	8.8	115.9
Nb	14	6.1	13.8	18.7	6.7	22.9	14.2	5.2	1.1	6.2	2.8	4.9	0	6	18.6	10.1	12.2	8.7	10.5	11.4	8.7	17.7	12.9	11.8
La	31	0	37.8	38.5	4	2.5	0	0	1.8	0	0	0.7	1.7	28	12.6	2	8	5	5.1	8.3	5.5	29.5	10.2	30.6
Ba	417.4	572.9	406.5	82.6	270.3	130.3	560.8	123	45.4	289.8	85.3	623.7	711.9	67.3	1400.8	1073.2	643.9	2023.8	590.2	414.4	1689.2	511.8	174.5	580.5

REFERENCES

REFERENCES

Ague, J. J., and van Haren, J. L. M., 1996, Assessing metasomatic mass and volume changes using the bootstrap, with application to deep crustal hydrothermal alteration of marble: Economic Geology, v. 91, p. 1169-1182.

Barovich, K. M., Patchett, P. J., Peterman, Z. E., and Sims, P. K., 1989, Nd isotopes and the origin of 1.9-1.7 Ga Penokean continental crust of the Lake Superior region: Geological Society of America Bulletin, v. 101, p. 333-338.

Baumgartner, L. P., and Olsen, S. N., 1995, A least-squares approach to mass transport calculations using the isocon method: Economic Geology, v. 90, p. 1261-1270.

Bell, T. H., and Cuff, C., 1989, Dissolution, solution transfer, diffusion versus fluid flow and volume loss during deformation/metamorphism: Journal of Metamorphic Geology, v. 7, p. 425-447.

Breithart, M. S., 1983, Significance of the distribution of clastic lenses within the Negaunee Iron Formation at the eastern end of the Palmer Basin, Marquette Synclinorium, Northern Michigan: Master's Thesis, Michigan State University.

Cambray, F. W., 1978, Plate tectonics as a model for the development of deposition and deformation of the early Precambrian (Precambrian X) of northern Michigan: Geological Society of America Abstracts with Programs, v. 10, p. 376.

Cambray, F. W., 1992, Detachment faulting associated with the deposition of the Lower Proterozoic Marquette Range Supergroup, northern Michigan: Geological Society of America Abstracts with Programs, v. 24, p. 93.

Cannon, W. F., 1973, The Penokean orogeny in Northern Michigan: The Geological Association of Canada Special Paper, no. 12, p. 251-271.

Cannon, W. F., and Simmons, G. C., 1973, Geology of part of the Southern Complex, Marquette district, Michigan: United States Geological Survey Journal of Research, v. 1, p. 165-172.

Chadwick, R. A., 1993, Aspects of basin inversion in southern Britain: Journal of the Geological Society, London, v. 150, p. 311-322.

Gair, J. E., and Simmons, G. C., 1968, Palmer Gneiss-an example of retrograde metamorphism along an unconformity: U. S. Geological Survey Professional Paper, 600-D, p. D186-D194.

Gillcrist, R., Coward, M., and Mugnier, J. L., 1987, Structural inversion and its controls: examples from the Alpine foreland and the French Alps: Geodinamica Acta (Paris), v. 1, p. 5-34.

Glazner, A. F., and Bartley, J. M., 1991, Volume loss, fluid flow and state of strain in extensional mylonites from the central Mojave Desert, California: Journal of Structural Geology, v. 13, p. 587-594.

Grant, J. A., 1986, The isocon method-A simple solution to Gresens' equation for metasomatic alteration: Economic Geology, v. 81, p. 1976-1982.

Gresens, R. L., 1967, Composition-volume relationships of metasomatism: Chemical Geology, v. 2, p. 47-65.

Hippertt, J. F., 1998, Breakdown of feldspar, volume gain and lateral mass transfer during mylonitization of granitoid in a low metamorphic grade shear zone: Journal of Structural Geology, v. 20, p. 175-193.

Hoffman, P. H., 1987, Early Proterozoic foredeeps, foredeep magnatism, and Superior-type iron formations of the Canadian Shield, *in* Kroner, A., ed, Proterozoic Lithospheric Evolution: Geodynamics Series, v. 17, p. 85-96.

Jackson, J. A., 1980, Reactivation of basement faults and crustal shortening in orogenic belts: Nature, v. 283, p. 343-346.

James, H. L., 1954, Sedimentary facies of iron-formation: Economic Geology, v. 49, p. 235-293.

James, H. L., 1955, Zones of regional metamorphism in the Precambrian of northern Michigan: Geological Society of America Bulletin, v. 66, p. 1455-1488.

Kerrich, R., Fyfe, W. S., Gorman, B. E., and Allison, I., 1977, Local modification of rock chemistry by deformation: Contributions to Mineralogy and Petrology, v. 65, p. 183-190.

Larue, D. K., 1981a, The Chocolay Group, Lake Superior region, U.S.A.: Sedimentologic evidence for deposition in basinal and platform settings on an Early Proterozoic craton: Geological Society of America Bulletin, v. 92, p. 417-435.

Larue, D. K., 1981b, The Early Proterozoic pre-iron-formation Menominee Group siliciclastic sediments of the southern Lake Superior region: Evidence for sedimentation in platform and basinal settings: Journal of Sedimentary Petrology, v. 51, p. 397-414.

Larue, D. K., 1983, Early Proterozoic tectonics of the Lake Superior region; Tectonostratigraphic terranes near the purported collision zone, *in* Medaris, L. G., Jr., ed., Early Proterozoic geology of the Great Lakes region: Geological Society of America Memoir 160, p. 33-47.

Larue, D. K., and Sloss, L. L., 1980, Early Proterozoic sedimentary basins of the Lake Superior region; Summary: Geological Society of America Bulletin, Part I, v. 91, p. 450-452.

Lin, C. P., 1969, Clastic lenses in the Negaunee Iron Formation at the Empire mine, Palmer, Michigan: Master's Thesis, Bowling Green State University.

Lister, G. S., and Snoke, A. W., 1984, S-C mylonites: Journal of Structural Geology, v. 6, p. 617-638.

Morey, G. B., 1983, Lower Proterozoic stratified rocks and the Penokean orogeny n east-central Minnesota, *in* Medaris, L. G., Jr., ed., Early Proterozoic geology of the Great Lakes region: Geological Society of America Memoir 160, p. 97-112.

Morey, G. B., 1993, Early Proterozoic epicratonic rocks, *in* Sims, P. K., ed., Precambrian; Conterminous U. S.: The Geology of North America Series, Geological Society of America, Boulder, Colorade, v. C-2, p. 47-56.

Morey, G. B., and Sims, P. K., 1976, Boundary between two Precambrian W terranes in Minnesota and its geological significance: Geological Society of America Bulletin, v. 87, p. 141-152.

Myers, G., 1984, Structural analysis of foliated Proterozoic metadiabase dikes in the Marquette-Republic region of Northern Michigan: Master's Thesis, Michigan State University.

O'Hara, K., 1988, Fluid flow and volume loss during mylonitization: An origin for phylllonite in an overthrust setting, North Carolina, U.S.A.: Tectonophysics, v. 156, p. 21-36.

Phillpotts, A. R., Gray, N. H., Carroll, M., Steinen, R. P., and Reid, J. B., 1997, The Electronic Total Station – A versatile, revolutionary new geological mapping tool: Journal of Geoscience Education, v. 45, p. 38-45.

Platt, J. P., 1984, Secondary cleavages in ductile shear zones: Journal of Structural Geology, v. 6, p. 439-442.

Platt, J. P., and Vissers, R., L., M., 1980, Extensional structures in anisotropic rocks: Journal of Structural Geology, v. 2, p. 397-410.

Ramsay, J. G., 1980, Shear zone geometry: a review: Journal of Structural Geology, v. 2, p. 83-99.

Ramsay, J. G., and Graham, R. H., 1970, Strain variation in shear belts: Canadian Journal of Earth Science, v. 7, p. 786-813.

Ramsay, J. G., and Wood, D. S., 1973, The geometric effects of volume change during deformation processes: Tectonophysics, v. 16, p. 263-277.

Ring, U., 1999, Volume loss, fluid flow, and coaxial versus noncoaxial deformation in retrograde, amphibolite facies shear zones, northern Malawi, east-central Africa: Geological Society of America Bulletin, v. 111, p. 123-142.

Scott, G. W., and Lukey, H. M., 1999, Geologic field trip to the Tilden Mine: 45th Annual Institute on Lake Superior Geology, Marquette, Michigan, Proceedings, p. 114-128.

Simpson, C., and Schmid, S. M., 1983, An evaluation of criteria to deduce the sense of movement in sheared rocks: Geological Society of America Bulletion, v. 94, p. 1281-1288.

Sims, P. K., Card, K. D., Morey, G. B., and Peterman, Z. E., 1980, The Great Lakes tectonic zone-A major crustal structure in central North America: Geological Society of America Bulletin, Part 1, v. 91, p. 690-698.

Sims, P. K., Schultz, K. J., Peterman, Z. E., and Van Schmus, W. R., 1993, Wisconsin magmatic terrane, *in* Sims, P. K., ed., Precambrian; Conterminous U.S.: The Geology of North America Series, Geological Society of America, Boulder, Colorado, v. C-2, p. 56-60.

Spry, A. H., 1969, Metamorphic textures: Pergamon Press, Oxford, 350 p.

Steinsund, P. I., 1995, StereoNet Version 3.0 for Windows, Geological Software, Tromso, Norway.

Twiss, R., J., and Moores, E., M., 1992, Structural Geology, W. H. Freeman and Company, 499 p.

Van der Pluijm, B. A., and Marshak, S., 1997, Earth Structure: *An introduction to Structural Geology and Tectonics*, WCB McGraw-Hill, 495 p.

Van Hise, C. R., and Bayley, W. S., 1895, The Marquette iron-bearing district of Michigan: U. S. Geological Survey Monograph 28, 608 p.

Van Schmus, W. R., 1976, Early and Middle Proterozoic history of the Great Lakes area, North America: Royal Society of London Philosophical Transactions, ser. A, v. 280, p. 605-628.

Weaver, T. L., 1994, The role of volume loss in the development of deformation fabrics in Proterozoic Metadiabase dikes in the Marquette-Republic region of Northern Michigan: Master's Thesis, Michigan State University.

Westjohn, D. B., 1990, Regional finite strain patterns in Proterozoic slates and quartzites: Implications for heterogeneous strain related to flexural slip folding in the Marquette Synclinorium: Ph. D. Thesis, Michigan State University.

White, S. H., Burrows, S. E., Carreras, J., Shaw, N. D., and Humphreys, F. J., 1980, On mylonites in ductile shear zones: Journal of Structural Geology, v. 2, p. 175-187.